JOURNAL OF GEOPHYSICAL RESEARCH, VOL. 113, D00F01, doi:10.1029/2008JD010023, 2008

Boundary layer aerosol chemistry during TexAQS/GoMACCS 2006: Insights into aerosol sources and transformation processes

T. S. Bates,[1,2] P. K. Quinn,[1,2] D. Coffman,[1] K. Schulz,[1] D. S. Covert,[2] J. E. Johnson,[2,1] E. J. Williams,[3,4] B. M. Lerner,[3,4] W. M. Angevine,[3,4] S. C. Tucker,[3,4] W. A. Brewer,[4] and A. Stohl[5]

Received 25 February 2008; revised 31 May 2008; accepted 1 July 2008; published 27 November 2008.

[1] The air quality and climate forcing impacts of atmospheric aerosols in a metropolitan region depend on the amount, composition, and size of the aerosol transported into the region; the input and removal of aerosols and aerosol precursors within the region; and the subsequent chemical processing in the atmosphere. These factors were studied in the Houston-Galveston-Gulf of Mexico region, aboard the NOAA R/V *Ronald H. Brown* during the Texas Air Quality Study and Gulf of Mexico Atmospheric Composition and Climate Study (TexAQS/GoMACCS 2006). The aerosol measured in the Gulf of Mexico during onshore flow (low radon concentrations indicating no contact with land for several days) was highly impacted by Saharan dust and what appear to be ship emissions (acidic sulfate and nitrate). Mean (median) mass concentrations of the total submicrometer and supermicrometer aerosol were 6.5 (4.6) μg m^{-3} and 17.2 (8.7) μg m^{-3}, respectively. These mass loadings of ''background'' aerosol are much higher than typically observed in the marine atmosphere and thus have a substantial impact on the radiative energy balance over the Gulf of Mexico and particulate matter (PM) loadings (air quality) in the Houston-Galveston area. As this background aerosol moved onshore, local urban and industrial sources added an organic rich submicrometer component (66% particulate organic matter (POM), 20% sulfate, 14% elemental carbon) but no significant supermicrometer aerosol. The resulting aerosol had mean (median) mass concentrations of the total submicrometer and supermicrometer aerosol of 10.0 (9.1) μg m^{-3} and 16.8 (11.2) μg m^{-3}, respectively. These air masses, with minimal processing of urban emissions contained the highest $SO_2/(SO_2 + SO_4^=)$ ratios and the highest hydrocarbon-like organic aerosol to total organic aerosol ratios (HOA/POM). In contrast, during periods of offshore flow, the aerosol was more processed and, therefore, much richer in oxygenated organic aerosol (OOA). Mean (median) mass concentrations of the total submicrometer and supermicrometer aerosol were 20.8 (18.6) μg m^{-3} and 7.4 (5.0) μg m^{-3}, respectively. Sorting air masses based on their trajectories and time over land provides a means to examine the effects of transport and subsequent chemical processing. Understanding and parameterizing these processes is critical for the chemical transport modeling that forms the basis for air quality forecasts and radiative forcing calculations.

Citation: Bates, T. S., et al. (2008), Boundary layer aerosol chemistry during TexAQS/GoMACCS 2006: Insights into aerosol sources and transformation processes, *J. Geophys. Res.*, *113*, D00F01, doi:10.1029/2008JD010023.

1. Introduction

[2] Scattering and absorption of solar radiation by atmospheric particles affect Earth's radiation budget [*Intergovernmental Panel on Climate Change (IPCC)*, 2007] and impair visibility [*Malm et al.*, 1994]. Aerosol particles also affect cloud properties (i.e., albedo, lifetime, extent, and precipitation) [*IPCC*, 2007] and human health [*Harrison and Yin*, 2000] and upon deposition can harm sensitive aquatic and terrestrial ecosystems [*Schindler et al.*, 1989]. The effective management of these climate and air quality issues requires model systems that accurately parameterize the basic chemical and dynamical processes (e.g., emissions, atmospheric mixing and transport, and

[1]Pacific Marine Environmental Laboratory, NOAA, Seattle, Washington, USA.
[2]Joint Institute for the Study of the Atmosphere and Ocean, University of Washington, Seattle, Washington, USA.
[3]Cooperative Institute for Research in the Environmental Sciences, University of Colorado, Boulder, Colorado, USA.
[4]Chemical Sciences Division, Earth Systems Research Laboratory, NOAA, Boulder, Colorado, USA.
[5]Department of Regional and Global Pollution Issues, Norwegian Institute for Air Research, Kjeller, Norway.

0148-0227/08/2008JD010023$09.00

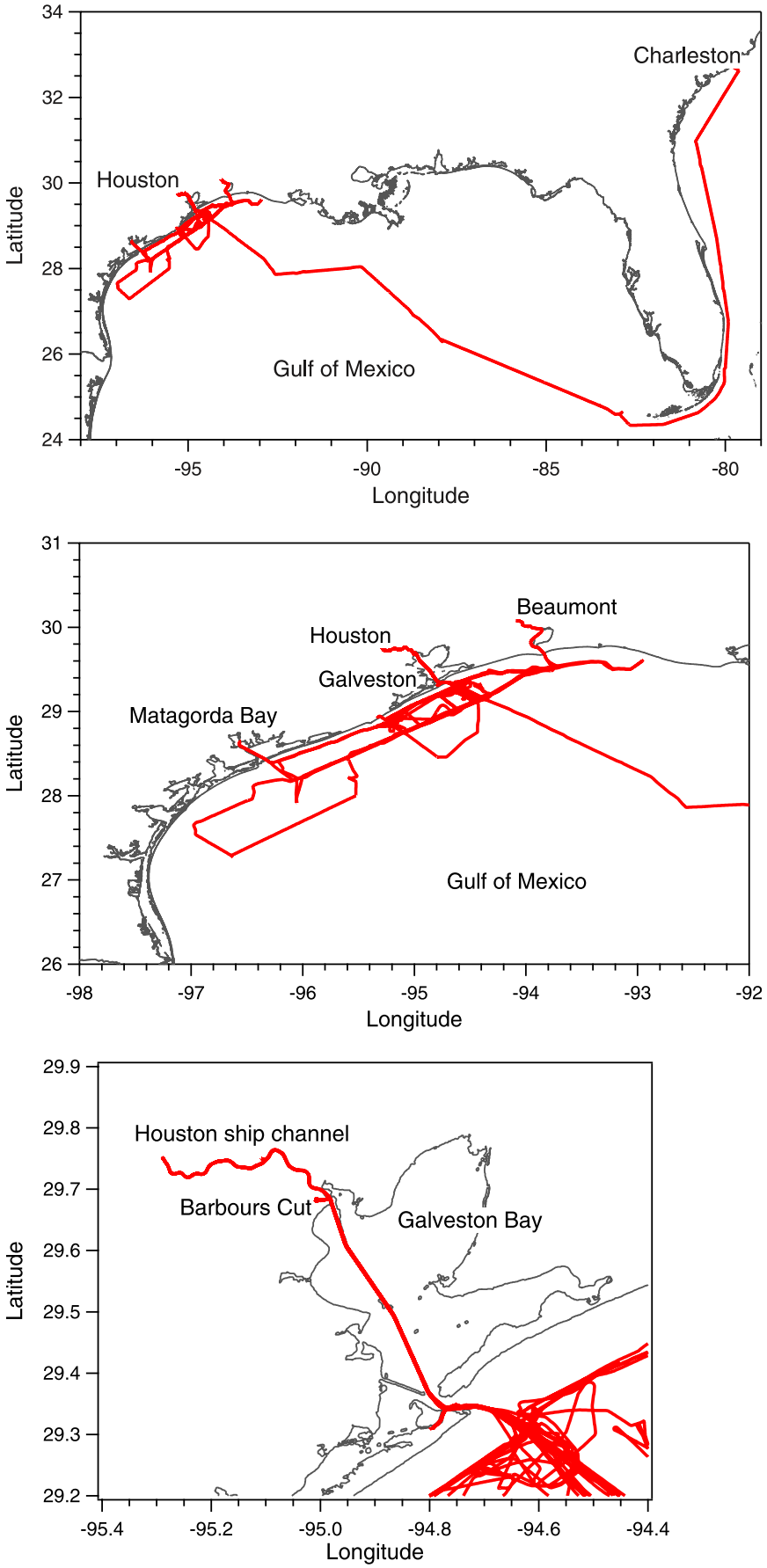
Charleston
Houston
Gulf of Mexico
Latitude
Longitude
Beaumont
Houston
Galveston
Matagorda Bay
Gulf of Mexico
Latitude
Longitude
Houston ship channel
Barbours Cut
Galveston Bay
Latitude
Longitude

Figure 1

chemical and physical transformations) that determine the atmospheric composition of aerosol particles and their precursors. The resulting calculated aerosol distributions must be evaluated against field measurements to identify the processes limiting model accuracy and to improve these model parameterizations. Reported here are aerosol distributions measured during the Texas Air Quality Study (TexAQS) and the Gulf of Mexico Atmospheric Composition and Climate Study (GoMACCS) aboard the NOAA R/V *Ronald H. Brown* (Figure 1). This intensive field study focused on providing a better understanding of the sources and atmospheric processes responsible for the formation and distribution of ozone and aerosols in the atmosphere and the influence that these species have on the regional radiative forcing of climate and air quality.

2. Methods

[3] The data reported here are available at http://saga.pmel.noaa.gov/data/. All references to time are reported here in CDST (UTC −5 h). Aerosol mass concentrations are reported as μg m^{-3} at STP (25°C and 1 atm).

2.1. Aerosol Sample Inlet

[4] Aerosol particles were sampled 18 m above the sea surface through a heated mast that extended 5 m above the aerosol measurement container. The mast was capped with a horizontal inlet nozzle that was rotated into the relative wind to maintain nominally isokinetic flow and minimize the loss of supermicrometer particles. Air entered the inlet through a 5 cm diameter hole, passed through a 7° expansion cone, and then into the 20 cm inner diameter sampling mast. The flow through the mast was 1 m^3 min^{-1}. The transmission efficiency for particles with aerodynamic diameters less than 6.5 μm (the largest size tested) is greater than 95% [*Bates et al.*, 2002].

[5] The bottom 1.5 m of the mast and the humidity controlled chamber containing the impactors, nephelometers, and sizing instruments were heated or cooled to establish a stable reference relative humidity (RH) for the sample air of ≈60%. A stable reference RH allows for constant instrumental size segregation in spite of variations in ambient RH and results in chemical, physical, and optical measurements which are directly comparable. In addition, measurement at a constant reference RH makes it possible, with the knowledge of appropriate growth factors, for end users of the data set (process, chemical transport, and radiative transfer models) to adjust the measured parameters to a desired relative humidity. A reference RH of 60% was chosen because it is above the crystallization humidity of most aerosol components and component mixtures [*Carrico et al.*, 2003]. For the atmospheric conditions encountered during TexAQS-GoMACCS 2006, it was possible to maintain the humidity controlled chamber at 58 ± 3.4% RH while heating the aerosol 2.5 ± 2.6°C (range −8 to +8°C) above the ambient temperature. The mean temperature in the chamber was 32.8 ± 1.4°C. For the continuous flow instruments discussed below (e.g., AMS, PILS-IC, PILS-WSOC, semicontinuous OC) the aerosol was heated for approximately 2 s.

2.2. Aerosol Chemical Composition

2.2.1. Impactor Sample Collection for Chemical Analysis

[6] Twenty one 1.6 cm outer diameter stainless steel tubes extended into the heated portion of the mast. These were connected to the aerosol instrumentation and impactors with conductive silicon tubing to prevent electrostatic loss of particles or stainless steel tubing for the lines to the impactors used for collection of carbonaceous aerosol and the aerosol mass spectrometer (AMS).

[7] The airflow to the impactors was controlled so that air was sampled only when the concentration of particles greater than 15 nm in diameter indicated the sample air was free of *Ronald H. Brown* emissions (i.e., there were no rapid increases in particle concentration), the relative wind speed was greater than 3 m s^{-1}, and the relative wind was forward of the beam.

[8] One- and two-stage multijet cascade impactors [*Berner et al.*, 1979] were used to determine submicrometer and supermicrometer concentrations of inorganic ions, organic and elemental carbon (OC and EC), and inorganic oxidized material (IOM). The 50% aerodynamic cutoff diameters of the impactors, $D_{50,aero}$, were 1.1 and 10 μm. The RH of the sampled air stream was measured a few inches upstream from the impactors. Throughout the paper submicrometer refers to particles with $D_{aero} < 1.1$ μm at 58 ± 3.4% RH and supermicrometer refers to particles with 1.1 μm < D_{aero} < 10 μm at 58 ± 3.4% RH. Sampling periods ranged from 2 to 14 h for all impactor samples. Blank levels were determined by loading an impactor with substrates but not drawing any air through it.

2.2.2. Impactor Sampling for Inorganic Ions

[9] Submicrometer and supermicrometer concentrations of Cl^-, NO_3^-, $SO_4^=$, methanesulfonate (MSA^-), Na^+, NH_4^+, K^+, Mg^{+2}, and Ca^{+2} were determined by ion chromatography (IC) [*Quinn et al.*, 1998]. Non-sea-salt sulfate concentrations were calculated by subtracting sea salt sulfate (based on Na^+ concentrations and the ratio of sulfate to sodium in seawater) from the total sulfate. Sea salt aerosol concentrations were calculated as

$$\text{sea salt } (\mu\text{g m}^{-3}) = \text{Cl}^- (\mu\text{g m}^{-3}) + \text{Na}^+(\mu\text{g m}^{-3}) \times 1.47 \quad (1)$$

where 1.47 is the seawater ratio of ($Na^+ + K^+ + Mg^{+2} + Ca^{+2} + SO_4^= + HCO_3^-$)/$Na^+$ [*Holland*, 1978]. This approach prevents the inclusion of non-sea-salt K^+, Mg^{+2}, Ca^{+2}, $SO_4^=$, and HCO_3^- in the sea salt mass and allows for the loss of Cl^- mass through Cl^- depletion processes. It also assumes that all measured Na^+ and Cl^- is derived from seawater.

Figure 1. R/V *Ronald H. Brown* cruise track during TexAQS-GoMACCS. The ship departed Charleston, South Carolina on 27 July 2006, arriving initially in Galveston, Texas on 2 August 2006. The cruise track included passages into Port Arthur/Beaumont, Matagorda Bay, Freeport Harbor, Galveston Bay to Barbour's cut (15 transits), and the Houston Ship Channel (four transits). The cruise ended in Galveston, Texas on 11 September 2006.

Results of *Savoie and Prospero* [1980] indicate that soil dust has a minimal contribution to measured soluble sodium concentrations.

[10] Sources of uncertainty in the ionic mass include the air volume sampled (±5%), the extract liquid volume (±3.3%), 2 times the standard deviation of the blank values measured over the course of the experiment, and the precision/calibration of the method (±5%). The average overall uncertainly in the total ionic submicrometer mass was ±8.5%.

2.2.3. Impactor Sampling for Organic and Elemental Carbon

[11] Submicrometer and sub-10 μm samples were collected using 2 and 1 stage impactors, respectively [*Bates et al.*, 2004]. A denuder was deployed upstream of the submicrometer impactor to remove gas phase organic species. OC and EC concentrations were determined with a Sunset Laboratory thermal/optical analyzer. The thermal program was the same as that used in ACE Asia [*Mader et al.*, 2003; *Schauer et al.*, 2003]. Four temperature steps were used to achieve a final temperature of 870°C in He to drive off OC. After cooling the sample down to 550°C, a He/O_2 mixture was introduced and the sample was heated in four temperature steps to 910°C to drive off EC. The transmission of light through the filter was measured to separate EC from any OC that charred during the initial stages of heating. No correction was made for carbonate carbon, so OC includes both organic and carbonate carbon.

[12] The mass of supermicrometer particulate organic matter (POM) was determined by multiplying the measured organic carbon concentration in μg m^{-3} by a factor of 2.0. The POM factor is an estimated average of the molecular weight per carbon weight and is based on a review of published measurements of the composition of organic aerosol in urban and nonurban regions [*Turpin and Lim*, 2001]. On the basis of the range of values given by *Turpin and Lim* [2001], the POM factor has an uncertainty of ±31%. Note that the submicrometer POM values reported here were obtained from the AMS, not the impactor samples (discussed further in section 3.2.1).

[13] The uncertainties associated with positive and negative artifacts in the sampling of semivolatile organic species can be substantial and are discussed below. Other sources of uncertainty in the POM mass include the air volume sampled (±5%), 2 times the standard deviation of the blanks measured over the course of the experiment, the precision/calibration of the method (±5%) based on the results of *Schauer et al.* [2003], and the POM factor (±31%). The average of the quadratic sum of these errors, ignoring positive and negative artifacts, yields an uncertainty of ±13% for OC and ±33% for POM.

[14] Sources of uncertainty in the EC mass include the air volume sampled (±5%) and the precision/calibration of the method (±13%) based on the results of *Schauer et al.* [2003]. A quadratic sum of these errors involved yields an uncertainty of ±14%.

2.2.4. Impactor Sampling for Inorganic Oxidized Material (Dust)

[15] Total elemental composition (Na, Mg, Al, Si, P, Cl, K, Ca, Ti, V, Cr, Mn, Fe, Ni, Cu, Zn, Ba, As, and Pb) was determined by thin-film X-ray primary and secondary emission spectrometry [*Bates et al.*, 2004]. A component composed of inorganic oxidized material (IOM) was constructed from the elemental data. The IOM most likely was composed of soil dust and/or fly ash. These two components are difficult to distinguish based on elemental ratios. To construct the IOM component, the mass concentrations of Al, Si, Ca, Fe, and Ti, the major elements in soil and fly ash, were combined. It was assumed that each element was present in the aerosol in its most common oxide form (Al_2O_3, SiO_2, CaO, K_2O, FeO, Fe_2O_3, TiO_2). The measured elemental mass concentration was multiplied by the appropriate molar correction factor as follows:

$$[\mathrm{IOM}] = 2.2[\mathrm{Al}] + 2.49[\mathrm{Si}] + 1.63[\mathrm{Ca}] + 2.42[\mathrm{Fe}] + 1.94[\mathrm{Ti}] \quad (2)$$

[*Malm et al.*, 1994; *Perry et al.*, 1997]. This equation includes a 16% correction factor to account for the presence of oxides of other elements such as K, Na, Mn, Mg, and V that are not included in the linear combination. In addition, the equation omits K from biomass burning by using Fe as a surrogate for soil K and an average K/Fe ratio of 0.6 in soil [*Cahill et al.*, 1986].

[16] Sources of uncertainty in the IOM mass concentration include the volume of air sampled (±5%), the area of the filter (±5%), 2 times the standard deviation of the blank values measured over the course of the experiment for each element, and the precision of the X-ray analysis [*Feely et al.*, 1991]. The average overall uncertainty in the IOM mass, propagated as a quadratic sum of the errors, was ±12%.

2.2.5. Impactor Sampling for Gravimetrically Determined Mass

[17] Films and filters were weighed at PMEL with a Cahn Model 29 and Mettler UMT2 microbalance, respectively [*Quinn and Coffman*, 1998]. The balances are housed in a glove box kept at a humidity of 65 ± 4%. The resulting mass concentrations from the gravimetric analysis include the water mass that is associated with the aerosol at 65% RH. The average uncertainty in submicrometer gravimetric mass, calculated as outlined by *Quinn et al.* [2000], was ±8.4%.

2.2.6. Aerodyne Mass Spectrometer Sampling of Nonrefractory Aerosol Composition

[18] Concentrations of submicrometer NH_4^+, $SO_4^=$, NO_3^-, and POM were measured with a quadrupole aerosol mass spectrometer (Q-AMS) (Aerodyne Research Inc., Billerica, Massachusetts, USA) [*Jayne et al.*, 2000]. The species measured by the AMS are referred to as nonrefractory (NR) and are defined as all chemical components that vaporize at the vaporizer temperature of ~550°C. This includes most organic carbon species and inorganic species such as ammonium nitrate and ammonium sulfate salts but not mineral dust, elemental carbon, or sea salt. The ionization efficiency of the AMS was calibrated every few days with dry monodisperse NH_4NO_3 particles using the procedure described by *Jimenez et al.* [2003]. The instrument operated on a 5 min cycle with the standard AMS aerodynamic lens.

[19] The POM aerosol was divided into two fractions, a hydrocarbon-like organic aerosol (HOA) and an oxygenated organic aerosol (OOA) using a multiple linear regression of the m/z 57 and m/z 44 signals, respectively (algorithm 1

[*Zhang et al.*, 2005]). The regression was conducted on the entire data set and the reconstructed organic concentrations (HOA + OOA) agreed well with the measured values (r^2 = 0.97, slope = 0.97). The regression coefficients determined in the AMS mass spectral mode were used to derive the HOA and OOA mass size distributions. A two-component analysis, as conducted here, can underrepresent [*Ulbrich et al.*, 2008] or overrepresent [*Lanz et al.*, 2007] the OOA fraction by up to 20% in cases where more than two components are needed to describe the data set. Although there was no evidence for a wood burning aerosol source (elevated concentrations of non-sea-salt potassium) in the study area, we do not equate HOA and OOA to primary or secondary organic aerosol as the direct emission of oxygenated aerosol species from sources like biomass burning, charbroiling, food cooking cannot be ruled out [*Lanz et al.*, 2007]. A more detailed positive matrix factorization of this data set will be presented in a subsequent manuscript.

[20] The collection efficiency of the AMS is the product of the transmission of particles through the aerodynamic lens (E_L), the efficiency with which particles are focused by the lens and directed to the vaporizer (E_s), and the degree to which particles are vaporized and analyzed versus bounced off the vaporizer (E_B) [*Huffman et al.*, 2005]. The AMS sampled downstream of an impactor with a 50% aerodynamic cutoff diameter of 1.1 μm. The collection efficiency of the aerodynamic lens, E_L, on the AMS inlet, however, is less than 1 for particles with aerodynamic diameters between 500 nm and 1 ìm [*Jayne et al.*, 2000]. Particle losses in this size range were corrected using a linear E_L collection efficiency curve (where E_L was equal to 100% at 550 nm and 10% at 1000 nm vacuum aerodynamic diameter). The correction added, on average, 14 ± 8% to the AMS total mass.

[21] The shape-related collection efficiency, E_S, depends on the efficiency with which particles are focused by the lens and directed to the vaporizer [*Jayne et al.*, 2000; *Huffman et al.*, 2005]. On the basis of beam width probe data, there was no indication that this factor was different from one for this data set. The collection efficiency due to particle bounce, E_B, appears to be a function of particle water content and chemical composition [*Allan et al.*, 2003]. The AMS sampling line coming from the humidity controlled chamber (58 ± 3.4% RH) was controlled to 52 ± 3.2% RH. Pure ammonium nitrate particles, used in the calibration of the instrument have an E_B of nearly 1 [*Jayne et al.*, 2000]. Particles with a high percentage of ammonium sulfate have an E_B of around 0.5 [*Allan et al.*, 2003; *Matthew et al.*, 2008]. An E_B of 0.5 is often used when no other chemical information is available. Comparison of the size corrected (E_L) AMS NR sulfate from this cruise with sulfate derived from a particle-into-liquid sampler coupled to an ion chromatograph (PILS-IC) suggests an E_B that varied from 1 for acidic sulfate (ammonium to sulfate molar ratio of <0.5) to 0.54 for ammonium sulfate. Therefore, E_B was assigned to each 5 min sample based on the AMS ammonium to sulfate molar ratio with E_B as an exponential function of the ammonium to sulfate molar ratio varying from 0.54 to 1 for ammonium to sulfate molar ratios of 2 to 0.5. There was no indication from the AMS mass size distributions that the ammonium to sulfate molar ratio varied as a function of size over the accumulation mode size range. A linear regression of 5 min transmission and bounce corrected AMS sulfate concentrations versus PILS-IC sulfate concentrations yielded a slope of 0.95 and an r^2 of 0.81. The uncertainty in the AMS concentration measurements during TexAQS/GoMACCS was estimated at ±20%.

2.2.7. PILS Sampling of Water Soluble Organic Carbon

[22] Water soluble organic carbon (WSOC) was measured with a particle-into-liquid sampler (PILS) [*Weber et al.*, 2001, *Orsini et al.*, 2003] coupled to a Sievers Model 800 Turbo Total Organic Carbon Analyzer [*Sullivan et al.*, 2006]. WSOC is operationally defined as the fraction of particulate organic carbon that is collected in water by the PILS and penetrates a 0.5 μm filter [*Sullivan et al.*, 2004]. The PILS sampled downstream of an impactor with a 50% aerodynamic cutoff diameter of 1.1 μm. A parallel plate carbon denuder was placed upstream of the PILS to remove gas phase organic compounds. The flow was split downstream of the denuder with a 15 l min^{-1} bypass flow and 15 l min^{-1} going to the PILS. The sample air was passed through a HEPA filter for 15 min every 45–120 min to remove particles and determine the measurement background. This measurement background was subtracted from the sample air to obtain WSOC concentrations. The water flow coming out of the PILS passed through a 0.5 μm in-line filter to remove particles. The system was standardized by running a dilute liquid sucrose sample through the PILS with the sample air passing through the HEPA filter. Dilution of the sample within the PILS was corrected by directly measuring the water flows through the debubbler, drain, and top of the PILS impactor. Data were recorded every 1 min. The WSOC relative uncertainty was estimated to be between ±20% based on the combined uncertainties associated with air (±5%) and liquid (±5%) flows, calibration (±5%) and background variability (±17%).

2.2.8. PILS Sampling of Inorganic Ions

[23] Inorganic ions were measured with a PILS coupled to two Metrohm Compact 761 ion chromatographs (IC) operated for the analysis of cations and anions [*Weber et al.*, 2001, *Orsini et al.*, 2003]. The PILS sampled downstream of an impactor with a 50% aerodynamic cutoff diameter of 1.1 μm. The flow was split downstream of the impactor with a 15 l min^{-1} bypass flow and 15 l min^{-1} going to two denuders (URG, Inc) located in series after the impactor and upstream of the PILS. One denuder was coated with sodium carbonate to remove gas phase acids and a second denuder was coated with phosphorous acid to remove gas phase bases. The sample air was periodically valved through a HEPA filter to remove particles and determine the measurement background. Samples were collected and analyzed every 5 min. The system was standardized by injecting standard solutions directly into the IC loops. Dilution of the sample within the PILS was corrected by directly measuring the water flows through the debubbler, drain, and top of the PILS impactor.

2.2.9. Sunset Laboratory Semicontinuous Sampling of Organic Carbon

[24] Organic carbon also was measured with a Sunset Laboratory real-time, semicontinuous thermal/optical carbon analyzer. The instrument sampled downstream of an

impactor with a 50% aerodynamic cutoff diameter of 1.1 μm and a parallel plate carbon denuder to remove gas phase organic compounds. The flow was split downstream of the denuder with a 21 l min^{-1} bypass flow and 9 l min^{-1} going to the carbon analyzer (filter face velocity = 97 cm s^{-1}). The instrument sampled air for 45 or 105 min depending on the OC concentrations. At the end of the sampling time the instrument analyzed the filter (15 min) using the same temperature program as the laboratory instrument described in section 2.2.3. The concentration of evolved CO_2 was measured with an NDIR detector. The sampling times were not sufficient to measure EC above the instrument detection limit (0.35 ìg m^{-3} based on a 45 min sample time). The sample air was periodically valved through a HEPA filter for the 45 or 105 min sampling time to remove particles and determine the measurement background. Sources of uncertainty for the real-time semicontinuous OC measurement include the air volume sampled (5%), the precision of the method (3%) based on injection of a CH_4 standard with each run, and the variability of the background signal (20%). The total uncertainty, excluding positive or negative artifacts, propagated as a quadratic sum of the errors was ±21%.

2.3. Ozone, Sulfur Dioxide, and Carbon Monoxide

[25] At the base of the sampling mast a 1.4 L min^{-1} flow was pulled through a 0.32 cm ID, 2 m long Teflon tube into a TECO 49 c ozone analyzer that had been calibrated to a NIST traceable analyzer at NOAA-GMD. Data were recorded in 10 s averages. The detection limit was 2 ppbv and the overall uncertainty was ±2 ppbv + 5%.

[26] Similarly, at the base of the sampling mast a 0.5 L min^{-1} flow was pulled through a 0.32 cm inner diameter, 1 m long Teflon tube, a Millipore Fluoropore filter (1.0-μm pore size) housed in a Teflon filter holder, a Perma Pure Inc. Nafion Drier (MD-070, stainless steel, 61 cm long) and then through 2 m of Telfon tubing to a Thermo Environmental Instruments Model 43C Trace Level Pulsed Fluorescence SO_2 Analyzer. The initial 1 m of tubing, filter, and drier were located in the humidity-controlled (60%) chamber at the base of the mast. Dry zero air (scrubbed with a charcoal trap) was run through the outside of the Nafion Drier at 1 $Lmin^{-1}$. Data were recorded in 10 s averages.

[27] Zero air was introduced into the sample line upstream of the Fluoropore filter for 10 min every 6 h to establish a zero baseline. An SO_2 standard was generated with a permeation tube (Vici Metronics, 21.6 ng S min^{-1} at 40°C). The flow over the permeation tube, diluted to 5.6 ppb, was introduced into the sample line upstream of the Fluoropore filter for 10 min every 24 h. The limit of detection for the 1 min data, defined as 2 times the standard deviation of the signal during the zero periods, was 100 ppt. Uncertainties in the concentrations based on the permeation tube weight and dilution flows was <5%.

[28] CO was measured with a modified AeroLaser GmbH (Garmisch-Partenkirchen, Germany) AL5002 Ultra-Fast CO analyzer, a commercially available vacuum-UV resonance fluorescence instrument [*Gerbig et al.*, 1999]. Ambient air was sampled from an inlet located approximately 16 m above waterline and 5 m starboard of the aerosol mast inlet; sample air was pulled through a 1.59 cm ID, 10 m long PFA manifold at a flow of 200 lpm to the instrument location. A 0.32 cm ID, 1 m long PFA tap delivered the sample to a Nafion drying tube, which reduced water vapor to less than 0.5 ppth. The CO analyzer then measured the dried air. Mixing ratios were reported for ambient air by correcting for the removed water vapor, using the water vapor mixing ratio measured at the inlet with a Vaisala RH probe. The water mixing ratio was typically 30 ppth (3%) during the campaign, and the correction was always less than 4%. Data were collected at 1 Hz and averaged to 1-min resolution; the total uncertainty was 3%, with a limit of detection of 1.5 ppbv.

2.4. Radon

[29] ^{222}Rn (half-life 3.82 days) was detected with a dual-flow loop two-filter detector [*Whittlestone and Zahorowski*, 1998]. The photomultiplier counted the radon daughters produced in the 750 L decay/counting tank with a lower limit of detection of 80 mBq m^{-3} for a 30 min count (with 30% error). The radon detector was standardized using radon emitted from a dry radon source (RN-25, Pylon Electronics Corp., 2850 mBq min^{-1}) following the procedures outlined by *Whittlestone and Zahorowski* [1998]. The background counts were measured with the airflow set to zero.

2.5. Number Size Distributions

[30] One of the 21 mast tubes was used to supply ambient air to a short column differential mobility particle sizer (Aitken-DMPS), a medium column differential mobility particle sizer (Accumulation-DMPS) and an aerodynamic particle sizer (APS, TSI model 3321). The two DMPSs were located in a humidity-controlled box (RH = 60%) at the base of the mast. The Aitken-DMPS was a short column University of Vienna [*Winklmayr et al.*, 1991] instrument connected to a TSI 3760A particle counter (TSI, St. Paul, Minnesota) operating with a positive center rod voltage to sample particles with a negative charge. Data were collected in 10 size bins from 20 to 200 nm geometric diameter. The Aitken-DMPS operated with an aerosol flow rate of 1 L $min^{-1}$and a sheath airflow rate of 10 L min^{-1}. The Accumulation-DMPS was a medium column University of Vienna instrument connected to a TSI 3760A particle counter operating with a positive center rod voltage to sample particles with a negative charge. The aerosol was charged with a Kr^{85} charge neutralizer (TSI model 3077) upstream of each DMA also at 60% RH. Data were collected in seven size bins from 200 to 800 nm diameter. The Accumulation-DMPS operated with an aerosol flow rate of 0.5 L $min^{-1}$and a sheath airflow rate of 5 L min^{-1}. The relative humidity of the sheath air for both DMPSs was controlled resulting in a measurement RH in the DMPSs of approximately 60%. With this RH control the aerosol should not have effloresced if it was hydrated in the atmosphere [*Carrico et al.*, 2003]. Mobility distributions were collected every 5 min.

[31] The mobility distributions were inverted to a number distribution assuming a Fuchs-Boltzman charge distribution from the charge neutralizer. The overlapping channels between the two instruments were eliminated in the inversion. The data were corrected for diffusional losses and size-dependent counting efficiencies. The estimated uncertainty in the number concentration in each bin, based on flow

uncertainties was ±10%. The DMPS data were converted from geometric diameters to aerodynamic diameters using calculated densities and the water masses associated with the inorganic ions at the measurement RH. The densities and associated water masses were calculated with a thermodynamic equilibrium model (AeRho) using the measured chemical data [*Quinn et al.*, 2002].

[32] The APS was located in the lower humidity controlled box (60% RH) at the base of the mast. The inlet to the APS was vertical and its sample withdrawn isokinetically from the larger flow to the DMPS. The APS was modified to minimize internal heating of the sample flow in the APS by its sheath flow and waste heat and thus maintain 60% RH [*Bates et al.*, 2005]. Number size distributions were collected with the APS every 5 min. The APS data were collected in 34 size bins with aerodynamic diameters ranging from 0.96 to 10.37 μm. The APS has been shown to underestimate the size of irregularly shaped particles, such as dust, by an average of 25% [*Marshall et al.*, 1991]. Since dust was a major component of the TexAQS/GoMACCS aerosol, the APS data were corrected for nonspherical particle shape using the dynamic shape factor (1.18) and ultra-Stokesian corrections of *Cheng et al.* [1993] as summarized by *Quinn et al.* [2004]. The estimated uncertainty in the supermicrometer size distribution was ±10%.

2.6. Seawater DMS

[33] Seawater entered the ship at the bow, 5.6 m below the ship waterline, and was pumped to the ship laboratory at approximately 30 lpm (water residence time within the ship was <5 min). Every 30 min, a 5 ml water sample was valved from the ship water line directly into a Teflon gas stripper. The sample was purged with hydrogen at 80 ml min^{-1} for 5 min. DMS and other sulfur gases in the hydrogen purge gas were collected on a Tenax filled trap held at −5°C. During the sample trapping period, 6.2 pmoles of methylethyl sulfide (MES) were valved into the hydrogen stream as an internal standard. At the end of the sampling/purge period the trap was rapidly heated to 120°C and the sulfur gases were desorbed from the trap, separated on a DB-1 megabore fused silica column held at 70°C, and quantified with a sulfur chemiluminesence detector. Between each water sample the system analyzed either a DMS standard or a system blank. The system was calibrated using gravimetrically calibrated DMS and MES permeation tubes. The precision of the analysis has been shown to be ±2% based on replicate analysis of a single water sample at 3.6 nM DMS.

2.7. Back Trajectories

[34] FLEXPART, a Lagrangian particle dispersion model [*Stohl et al.*, 1998; *Stohl and Thomson*, 1999], was used to determine the origin of aerosols that had undergone transport to the ship. FLEXPART was driven with model-level data from the European Centre for Medium-Range Weather Forecasts (ECMWF) at a resolution of 0.36° × 0.36° in the area of interest here. The ECMWF model has four levels in the lowest 100 m of the atmosphere and can resolve some of the structure of the marine boundary layer. Backward simulations, as described by *Seibert and Frank* [2004], were done along the ship track every hour. Every simulation consisted of 40,000 particles released in the volume of air sampled. The backward simulations are done with full turbulence and convection parameterizations. The primary output of FLEXPART is an emission sensitivity, which indicates where and when emissions could have impacted the sampled air mass. The impact of surface emissions on the sampled air mass, for instance, is proportional to the local product of the emission strength and the emission sensitivity at the lowest altitude (the so-called footprint). For the purpose of classifying air masses according to their origin, the emissions sensitivity fields can be interpreted analogous to traditional air mass back trajectories.

2.8. Calculations of Aerosol Water Content

[35] The chemical thermodynamic equilibrium model AeRho was used to estimate the water mass associated with the inorganic ions at 60% RH and at ambient humidity. It was assumed that the inorganic aerosol was an internal mixture containing all measured ionic species. The chemical reactions included in the model, the crystallization humidities used for the solid phase species, and the method for the calculation of the aerosol water content are given by *Quinn et al.* [2002]. Both the IOM and the organic mass were assumed to not take up any water. AeRho was also used to calculate the refractive index and density for each chemical component based on measured size distributions and chemical composition. To check for internal consistency in the measured and modeled parameters, closure experiments were performed for measured and calculated mass (summarized in section 3.1.3).

2.9. Calculations of Mixing Height

[36] Mixing heights were calculated using velocity and aerosol data acquired from NOAA's High Resolution Doppler Lidar (HRDL), a 2 μm wavelength, motion stabilized, scanning, coherent, Doppler lidar that provides velocity and signal strength estimates with 30 m line-of-sight range resolution and an update rate of 2 Hz [*Grund et al.*, 2001]. Processing of velocity and backscatter data from various scan sequences provided high vertical resolution (5–30 m) profiles of horizontal mean wind speed and direction, and 30 m vertical resolution profiles of both atmospheric velocity variance and uncalibrated aerosol backscatter. A new set of profiles was acquired once every 15 min during the experiment. In this application, mixing height is defined as the top of the layer in turbulent connection with the surface. For most of the experiment, mixing height was estimated directly from turbulence profiles (S. C. Tucker et al., manuscript in preparation, 2008) by searching for the height in the variance profiles at which surface-connected turbulence dropped below the threshold of 0.04 m^2/s^2 (20 cm/s). Hourly averages of the mixing heights were used in this study.

3. Results and Discussion

3.1. Regional Aerosol Chemical Composition

3.1.1. Air Mass Categories

[37] The Azores High dominated the study region during most of August bringing southeasterly flow into the Gulf of Mexico. FLEXPART back trajectories showed that the air masses sampled at the ship had been over the Atlantic Ocean during the previous week, occasionally passing over

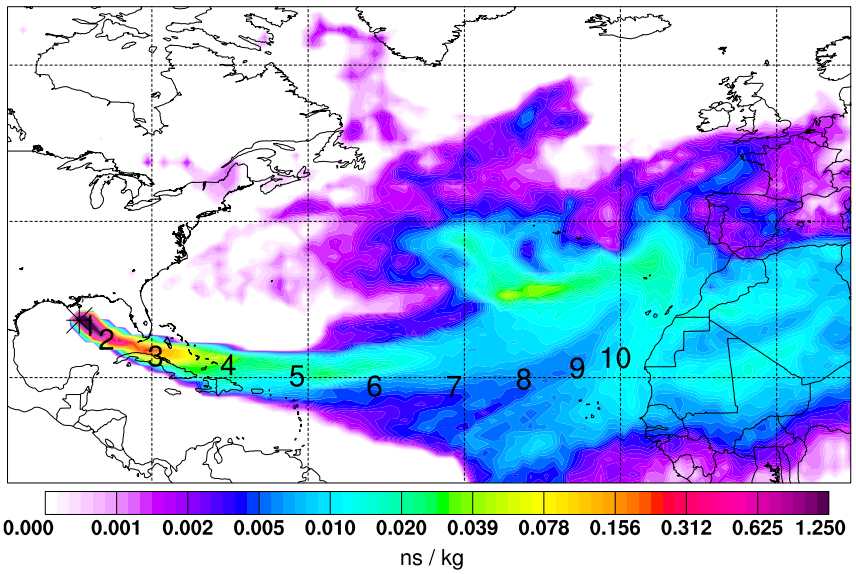

Figure 2. Flexpart footprint emission sensitivity showing transport to the Gulf of Mexico from Africa. The air mass sampled at the ship on 1 August 2006 had surface contact over the African continent 2 weeks prior. The superimposed numbers are the air mass centroid positions in daily intervals, for the last 10 days.

North Africa (Figure 2). Weather conditions during September were controlled by the local synoptic meteorology. Winds were generally light and variable with land/sea breezes established during the night/day. The dominant flow was from the north.

[38] A goal of this study was to characterize the regional aerosol chemical composition and the factors controlling this composition. Categorizing the aerosol data by source region, however, was complicated by the light, variable, and recirculating winds. In analyzing the data, three source categories emerged. We use Flexpart back trajectories, atmospheric radon measurements, and ship position to define these three categories. Category 1 (35% of the data) was defined by southerly (ESE to WSW) trajectories with the ship in the Gulf of Mexico. The mixing height of the marine boundary averaged 540 ± 140 m with no diurnal cycle. Low (generally <500 mBq m^{-3}) radon values indicated that the air mass had been over the water for several days. Thus category 1 was the "background" aerosol advecting into North America. Category 2 (39% of the data) was defined by the same trajectory and low radon values but with the ship sampling inland from the Gulf (e.g., Galveston Bay, Houston Ship Channel, Matagorda Bay, Beaumont). This constitutes the "background" aerosol with the addition of local sources. The boundary layer mixing heights for category 2 varied diurnally with a very shallow stable layer (200–300 m) at night and convective mixing to ≈800 m during the day. Category 3 (26% of the data) was defined by northerly (WNW to ENE) trajectories. Radon concentrations ranged from 1000 to 10,000 mBq m^{-3} indicating that the air mass had recently been over the continent. The boundary layer mixing heights for category 3 also varied diurnally when the ship was close to land with a very shallow stable layer (100–300 m) at night and con-

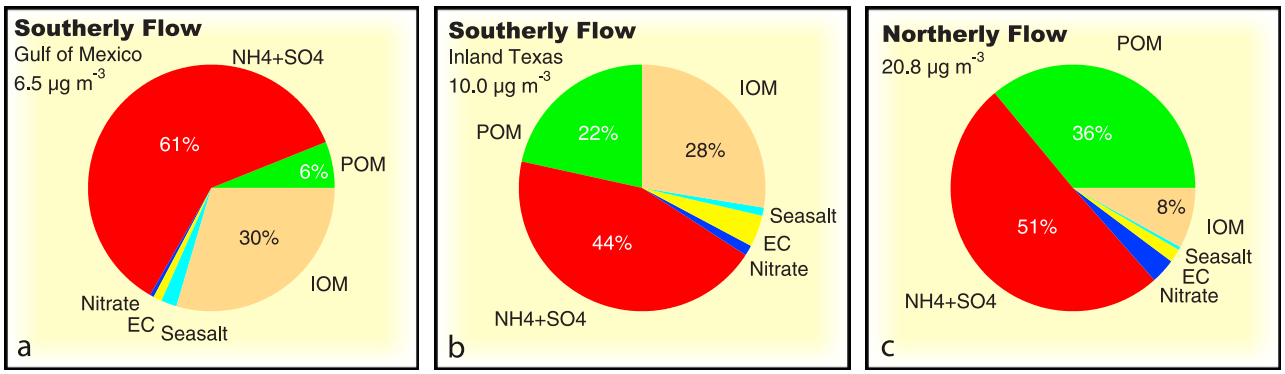

Figure 3. Submicrometer aerosol composition for (a) air masses sampled over the Gulf of Mexico during southerly flow (low radon concentrations), (b) air masses sampled within Texas (ports and harbors) during southerly flow (low radon concentrations), and (c) air masses sampled during northerly flow (high radon concentrations). The percentages are calculated as the average of the mass fractions for each sample. Consequently, the percentages are not equivalent to the mass fractions that could be calculated from the average concentrations (Table 2).

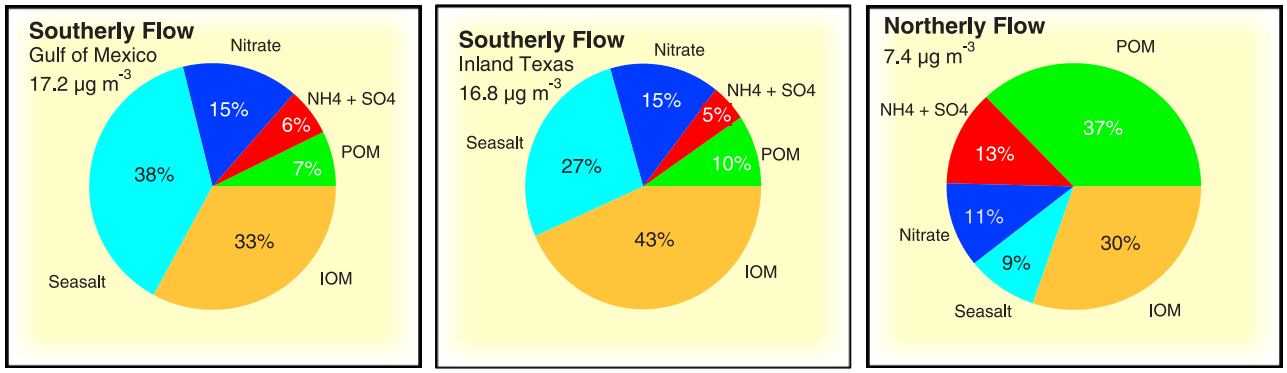

Figure 4. Supermicrometer aerosol composition during conditions defined in Figure 3.

vective mixing to ≈1200 m during the day. Offshore, the mixings heights averaged 540 m at all times of the day.

3.1.2. Submicrometer Aerosol Composition

[39] The submicrometer aerosol advecting into North America (category 1) was predominantly NR-NH_4^+ + NR-$SO_4^=$, (61 ± 23%) with an ammonium to sulfate molar ratio of 0.79 ± 0.42 (Figure 3). The air mass was highly impacted by IOM which made up 30 ± 26% of the dry aerosol (defined here as the sum of the chemically analyzed mass) submicron mass (6.5 ± 5.0 μg m^{-3}). This IOM was most likely Saharan dust based on calculated back trajectories and elemental ratios. The third most abundant component, NR-POM, comprised only 6.1 ± 4.8% of the total mass and was highly oxidized with an OOA/NR-POM ratio of 0.87. This ratio is between the Northern Hemisphere average "urban downwind" (83%) and "rural/remote" (95%) values reported by *Zhang et al.* [2005], suggesting some local influence of HOA.

[40] As the Gulf of Mexico "background" aerosol advected into Texas, the mean dry mass increased from 6.5 ± 5.0 μg m^{-3} to 10.0 ± 5.2 μg m^{-3} (Table 2). The submicrometer aerosol was still predominantly NR-NH_4^+ + NR-$SO_4^=$ (44 ± 17%) and IOM (28 ± 24%) but now included a much larger NR-POM fraction (22 ± 14%) (Figure 3). By difference, the added aerosol was predominantly NR-POM (66%), NR-NH_4^+ + NR-$SO_4^=$ (20%), and EC (14%). Adding this urban and industrial component resulted in an aerosol that was much less acidic (ammonium to sulfate molar ratio of 1.55 ± 0.60) and a NR-POM fraction that was much less oxidized (OOA/NR-POM ratio of 0.60) than the "background" aerosol.

[41] Submicrometer aerosol concentrations were highest during northerly flow (category 3) averaging 21 ± 11 μg m^{-3}. The aerosol was predominantly NR-NH_4^+ + NR-$SO_4^=$ (51 ± 16%) and NR-POM (36 ± 14%). The ammonium to sulfate molar ratio was similar to the category 2 aerosol (1.63 ± 0.54) but the NR-POM was much more oxidized (OOA/NR-POM ratio of 0.90).

3.1.3. Supermicrometer Aerosol Composition

[42] The supermicrometer aerosol advecting into North America (category 1) was predominantly sea salt (38 ± 13%) and dust (33 ± 24%) (Figure 4). With an ammonium to sulfate molar ratio of only 0.16, the sulfate (6.2 ± 2.5%) and nitrate (15 ± 11%) were likely associated with the sea

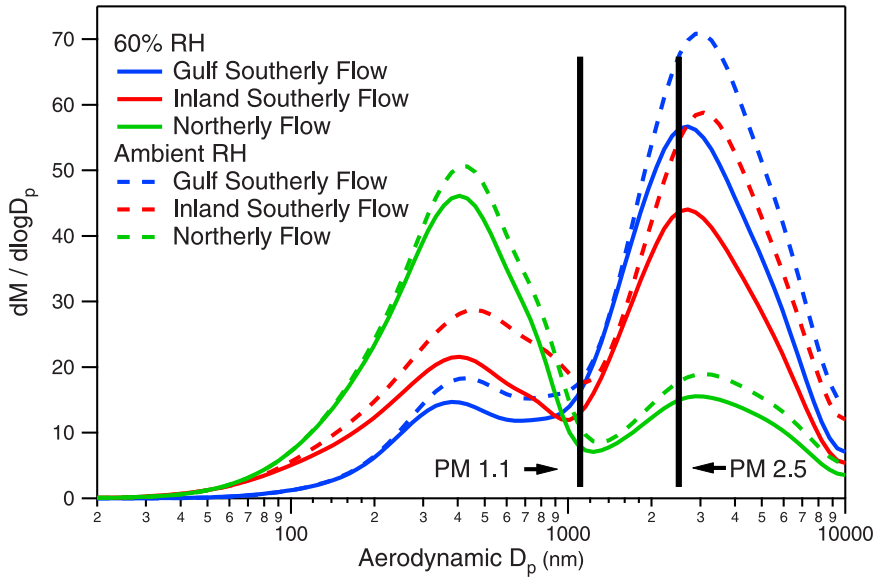

Figure 5. Aerosol mass size distributions during conditions defined in Figure 3 at the sampling relative humidity (RH) (60%) and adjusted to ambient RH.

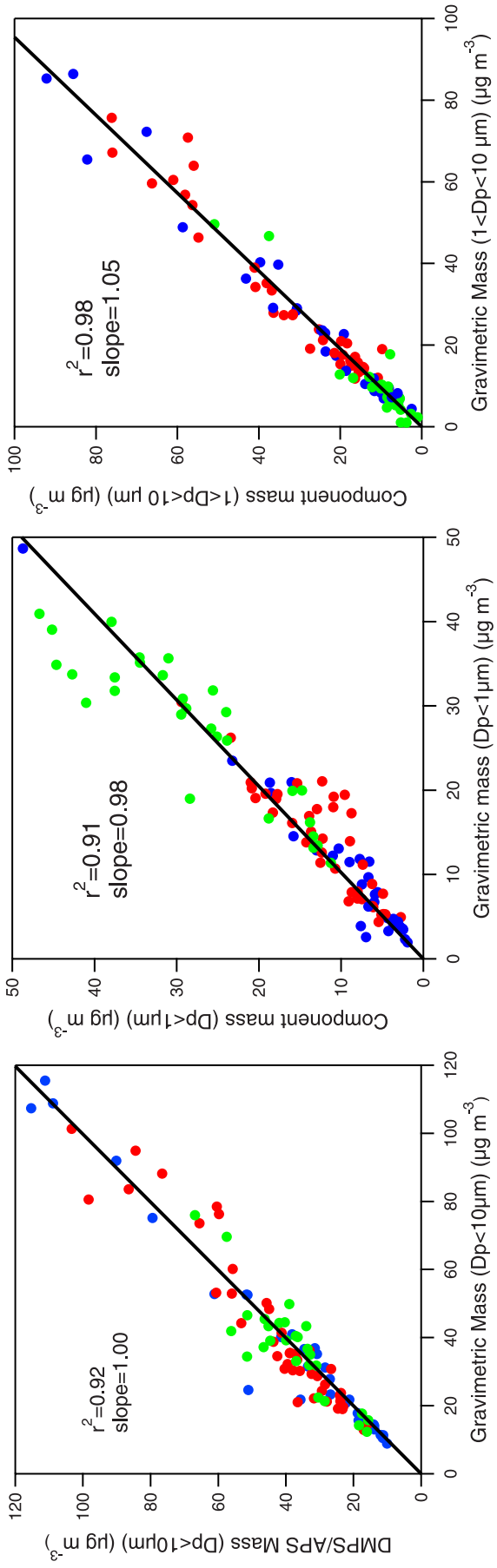

Figure 6. Mass closure between component mass (components shown in Figures 3 and 4 plus associated water at 60% RH), gravimetric mass, and number size distribution derived mass. The points are colored by air mass categories (section 3.1.1) where blue represents category 1, red represents category 2, and green represents category 3.

Table 1. Mean Aerosol Mass Concentrations for the Submicrometer, Supermicrometer, and PM2.5 Size Ranges in the Three Regions Described in Section 3.1[a]

		Category 1		Category 2		Category 3	
	Relative Humidity	Mean	Standard Deviation	Mean	Standard Deviation	Mean	Standard Deviation
			Submicrometer				
Component	dry	6.8	5.0	10.2	5.4	21.2	11.4
Component plus water	60%	10.7	9.7	14.6	7.0	34.5	13.2
Gravimetric	60%	10.0	9.2	13.5	6.5	27.5	8.8
Calculated	60%	8.0	4.3	14.2	13.4	28.2	16.7
			Supermicrometer				
Component	dry	17.2	21.5	16.8	12.7	7.4	8.1
Component plus water	60%	37.5	42.9	29.9	19.7	10.5	10.3
Gravimetric	60%	34.7	40.0	28.3	19.5	10.5	11.3
Calculated	60%	36.4	34.3	28.3	20.6	11.6	12.4
			PM 2.5				
Calculated	60%	17.3	11.0	21.6	15.2	31.4	17.1
Calculated	ambient	20.2	12.0	27.8	23.1	34.7	20.4

[a]Mean aerosol mass concentrations are measured in μg m^{-3} ($\pm 1\sigma$ standard deviation). Gravimetric denotes the gravimetrically analyzed mass; component is the sum of the mass analyzed for inorganic ions, particulate organic matter, inorganic oxidized material, and elemental carbon; component plus water includes the water calculated to be associated with the inorganic ions at 60% relative humidity; calculated denotes the mass estimated from the number size distribution and the density based on the measured chemical composition.

salt or dust. The average supermicrometer dry mass (17.2 ± 21 μg m^{-3}) was 3 times higher than the category 1 submicrometer aerosol. The category 2 supermicrometer aerosol was very similar to category 1 with slightly higher concentrations of nitrate and POM (Figure 4).

[43] Under northerly flow the supermicrometer aerosol concentrations (7.4 ± 8.2 μg m^{-3}) were only 1/3 of the submicrometer aerosol concentrations. The dominant aerosol component was POM (37 ± 20%) followed by IOM (30 ± 21%), sulfate (13 ± 11%), nitrate (11 ± 8%), and sea salt (9 ± 11%).

3.1.4. PM2.5 Mass

[44] Air quality regulations in the United States are based on aerosol mass concentrations of particles with diameters less than 2.5 μm. The aerosol sampling system deployed on *Ronald H. Brown* during TexAQS/GoMACCS used impactors, with a 50% aerodynamic cutoff diameter at 1.1 μm at 60% RH, to separate and sample the two dominant mass modes of the aerosol size distribution, the accumulation, and coarse modes (Figure 5). It is instructive to study these modes separately as they differ in sources, chemical composition (see above), removal mechanisms, optical properties, and health effects. Conducting measurements at a constant RH also facilitates comparisons of the aerosol mass determined by different methods (mass closure) which can be used to assess measurement/model uncertainties. Ultimately, these measurements can be used to calculate PM2.5 mass at a fixed RH or at ambient RH if mass closure can be demonstrated.

[45] Submicrometer and supermicrometer aerosol mass concentrations during TexAQS/GoMACCS were determined gravimetrically, by summing the chemically analyzed species, and from the number size distribution using the density of the total aerosol mixture estimated with AeRho. The amount of water associated with the aerosol at 60% RH was added to the chemically analyzed mass for comparison with the other methods. As shown in Figure 6 and Table 1, the mass concentrations from the three methods agreed

Table 2. Mean Aerosol Component Mass Concentrations for the Submicrometer and Supermicrometer Size Ranges in the Three Regions Described in Section 3.1[a]

	Category 1		Category 2		Category 3	
	Mean	Standard Deviation	Mean	Standard Deviation	Mean	Standard Deviation
			Submicrometer			
$NH_4^+ + SO_4^=$	3.0	1.3	4.2	2.9	9.8	6.2
NO_3^-	0.035	0.045	0.14	0.17	0.70	1.1
Sea salt	0.13	0.13	0.11	0.067	0.088	0.091
OOA	0.30	0.33	1.2	1.6	6.8	4.2
HOA	0.080	0.13	0.88	1.6	1.3	2.6
EC	0.075	0.064	0.42	0.31	0.38	0.23
IOM	3.5	5.6	3.1	3.8	1.3	2.0
			Supermicrometer			
$NH_4^+ + SO_4^=$	0.82	0.82	0.66	0.36	0.62	0.52
NO_3^-	1.4	1.0	1.8	1.0	0.72	0.90
Sea salt	5.4	5.4	3.6	2.1	0.56	0.78
POM	0.64	0.97	1.4	1.6	2.3	1.8
IOM	9.0	14	9.3	10	3.2	6.3

[a]Mean aerosol component mass concentrations are measured in μg m^{-3} ($\pm 1\sigma$ standard deviation). OOA, oxygenated organic aerosol; HOA, hydrocarbon-like organic aerosol; EC, elemental carbon; IOM, inorganic oxidized material; POM, particulate organic matter.

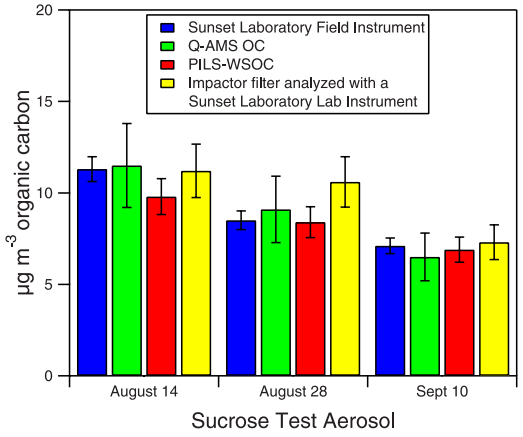

Figure 7. Mass closure between the four techniques used to measure organic aerosol. The comparisons were conducted using a soluble, nonvolatile ammonium sulfate/sucrose aerosol. The error bars indicate the uncertainty calculated for each technique (see section 2).

within the overall uncertainty of the closure experiment (26%, calculated from a quadrature sum of the uncertainties from each of the three methods). This supports our calculations of mass concentrations for different size classifications.

[46] The PM2.5 mass was calculated from the mass size distribution (Figure 5). Note that this size cut included a large fraction of the coarse mode aerosol which was a significant part (30–40%) of the PM2.5 mass during southerly flow (Table 1). The U.S. Environmental Protection Agency (EPA) has an annual mean standard of 15 μg m^{-3} for PM 2.5. If the measurements during the August/September 2006 campaign of TexAQS/GoMACCS are representative of the whole year, the Galveston/Houston region violates the standard based solely on the air coming into Texas under southerly flow.

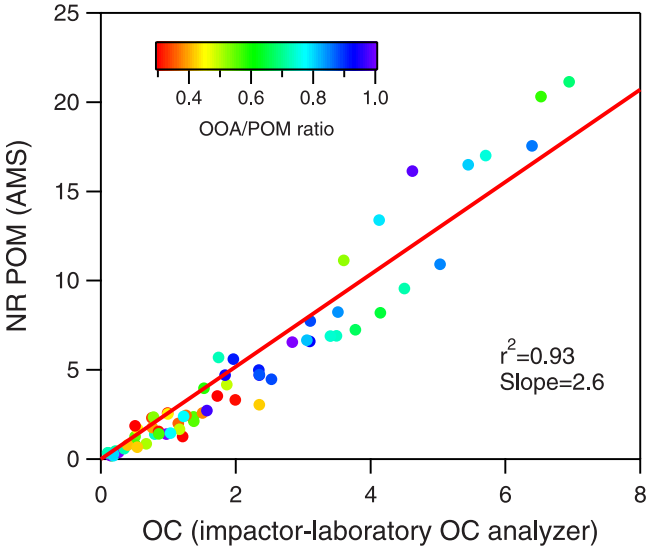

Figure 8. Correlation between nonrefractory (NR) particulate organic matter (POM) (aerosol mass spectrometer (AMS)) and nonvolatile organic carbon (impactor sampling/Sunset Laboratory thermal/optical carbon analyzer) concentrations. The data are colored by their oxygenated organic aerosol (OOA)/POM ratio.

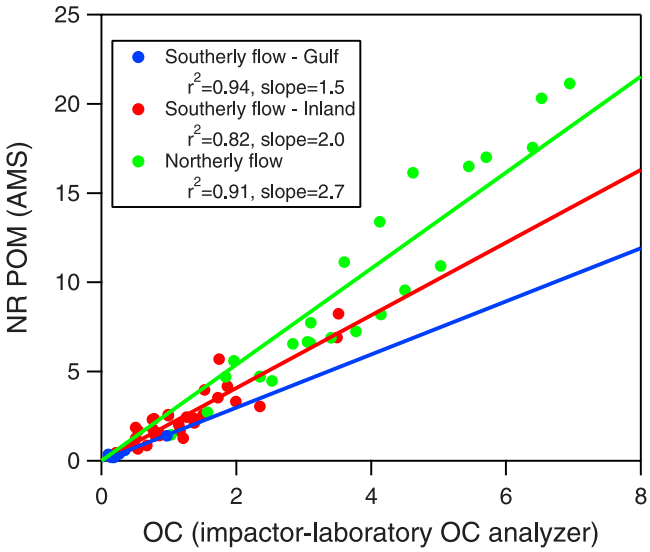

Figure 9. Correlation between NR POM (AMS) and nonvolatile organic carbon (impactor sampling/Sunset Laboratory thermal/optical carbon analyzer) concentrations. Data are separated into the conditions defined in Figure 3.

3.2. Regional Aerosol Characteristics and Sources

3.2.1. Organic Aerosol

[47] Atmospheric organic aerosol is comprised of many different compounds with a range of solubilities and volatilities [*Fuzzi et al.*, 2006]. This complexity leads to measurements of total organic aerosol that are operationally defined by the measurement technique. Organic aerosol was measured aboard *Ronald H. Brown* during TexAQS/GoMACCS using four different instruments: nonrefractory particulate organic matter (NR-POM) was measured with a quadrupole Aerodyne mass spectrometer (Q-AMS), particulate organic carbon (OC) was measured with two Sunset Laboratory thermal combustion organic/elemental carbon analyzers (laboratory and online), and water soluble organic carbon (WSOC) was measured with a particle-into-liquid sampler (PILS) coupled to a Sievers total carbon analyzer. A soluble, nonvolatile ammonium sulfate/sucrose aerosol was generated and fed into the sampling mast. Sucrose concentrations measured by the four techniques (Figure 7) agreed to within 11% (Q-AMS corrected for collection efficiency based on PILS-IC sulfate measurements). This was well within the uncertainties of the four techniques and demonstrated that the instrument inlets and calibrations were correct.

[48] The ambient Gulf of Mexico/Houston Area organic aerosol, however, contained nonsoluble and volatile components. The filters downstream of the 1 and 10 μm impactors, sampling at 30 L m^{-1}, had a filter face velocity of 52 cm s^{-1} while the online OC analyzer, sampling at 8.9 L m^{-1}, had a filter face velocity of 97 cm s^{-1}. The filter temperatures in both sampling systems were similar. A linear regression between samples from the online OC analyzer and the impactor/laboratory OC analyzer yielded an r^2 of 0.91 and a slope of 0.64 with the online OC analyzer

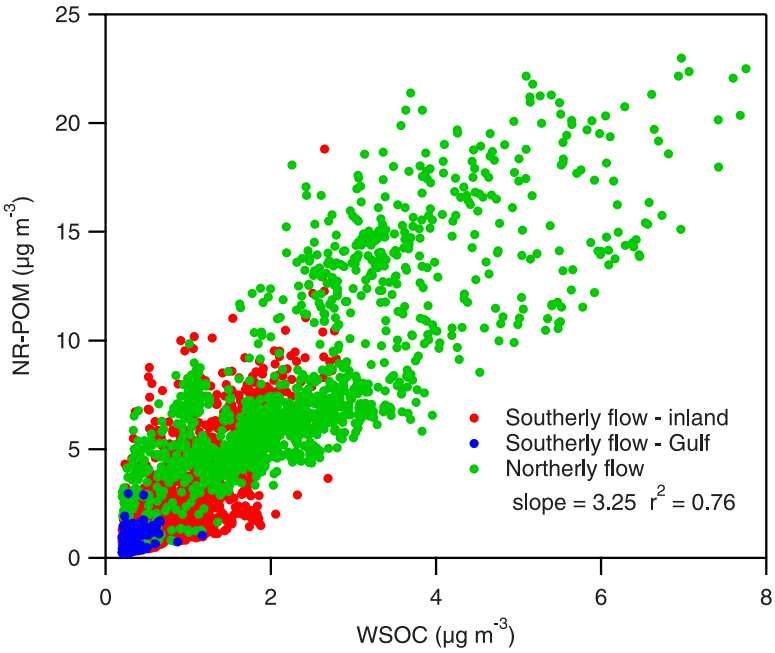

Figure 10. Correlation between and NR POM and water soluble organic compound.

results consistently less than the impactor/laboratory OC analyzer. As both sampling systems used identical denuders with flows of 30 L m^{-1}, we conclude that the lower values obtained with the online OC analyzer were due to a higher loss of semivolatile organic carbon (SVOC) from the filter during sampling. Similar losses have been documented by *Eatough et al.* [2003]. Attempts to quantify the SVOC downstream of the online OC analyzer filter were unsuccessful (carbon impregnated filter downstream of the particle filter). This may be in part due to the very high concentrations of VOCs in this area [*Jobson et al.*, 2004]. If the denuders passed even 1% of the VOCs, the signal measured as SVOC downstream of the OC filter would be much greater than the particulate OC.

[49] A linear regression between NR-POM and OC (impactor/laboratory OC analyzer) concentrations yielded an r^2 of 0.93 and a slope of 2.6 (Figure 8). This NR-POM/OC ratio is higher than typically observed in urban or rural areas (1.6 to 2.0 [*Turpin and Lim*, 2001]) and indicates either a highly oxidized aerosol or a loss of SVOC during impactor sampling. Samples with a high NR-POM/OC ratio did not necessarily have a high OOA/NR-POM ratio (Figure 8) and the OOA/NR-POM ratios reported here are very similar to that found in other areas of the Northern Hemisphere [*Zhang et al.*, 2007]. The highest NR-POM/OC ratios were found in the samples collected during northerly flow (Figure 9) when the ship was located in the Houston Ship Channel very close to industrial sources of organic gases. The loss of OC from these samples during denuder/filter sample collection is consistent with gas-particle partitioning of secondary organic aerosol (SOA) and has been discussed previously by *Eatough et al.* [2003]. SOA forms from the condensation of semivolatile reaction products of gas phase precursors. This partitioning is a reversible process as has been shown in the formation and evaporation of SOA from α-pinene [*Grieshop et al.*, 2007]. SOA can also form when semivolatile primary organic aerosol evaporates, oxidizes, and recondenses in the atmosphere [*Robinson et al.*, 2007]. This partitioning and photochemical processing creates a regionally distributed organic aerosol as opposed to readily defined plumes from distinct sources. This partitioning also leads to negative artifacts in traditional denuder/filter sampling. We hypothesize that the high NR-POM/OC ratios observed in this study region are a result of reevaporation of the SVOC from the filter.

[50] A NR-POM/OC ratio can also be estimated based on the AMS data alone [*Aiken et al.*, 2008]. Using the m/z of 44 as a surrogate for the oxygen content of POM and the m/z 44, POM, OC relationships described by *Aiken et al.* [2008], the NR-POM/OC ratio during TexAQS averaged 1.86 ± 0.17. This ratio is typical of that found in urban and rural areas [*Turpin and Lim*, 2001].

[51] A linear regression between NR-POM and WSOC concentrations yielded an r^2 of 0.76 and a slope of 3.2 (Figure 10). Correlations of OOA and HOA with WSOC yielded r^2 values of 0.67 and 0.15 and slopes of 2.6 and 0.47, respectively. The NR-POM/WSOC slope of 3.2 is very similar to that reported for the Gulf of Maine (3.3) [*de Gouw et al.*, 2007] and the OOA/WSOC slope of 2.6 is slightly less than that reported for Tokyo (3.2) [*Kondo et al.*, 2007]. With a NR-POM/OC ratio of 1.6 to 2.0 [*Turpin and Lim*, 2001], 49–62% of the NR-POM was water soluble. This is within the range of values (48–77%) measured during the summer months in other areas [*Zappoli et al.*, 1999; *Decesari et al.*, 2001; *Sullivan et al.*, 2004; *Jaffrezo et al.*, 2005] With an OOA/OC ratio of 2.2 [*Zhang et al.*, 2005; *Kondo et al.*, 2007], 85% of the OOA was water soluble during TexAQS/GoMACCS.

[52] The diurnal cycles of HOA and OOA concentrations provide insights into the processes controlling their concentrations in the boundary layer. HOA concentrations have been shown to correlate with CO mixing ratios [*Allan et al.*, 2003; *Zhang et al.*, 2005] and other markers of automobile exhaust emissions. Although this correlation was weak in the Galveston/Houston region ($r^2 = 0.19$) presumably from

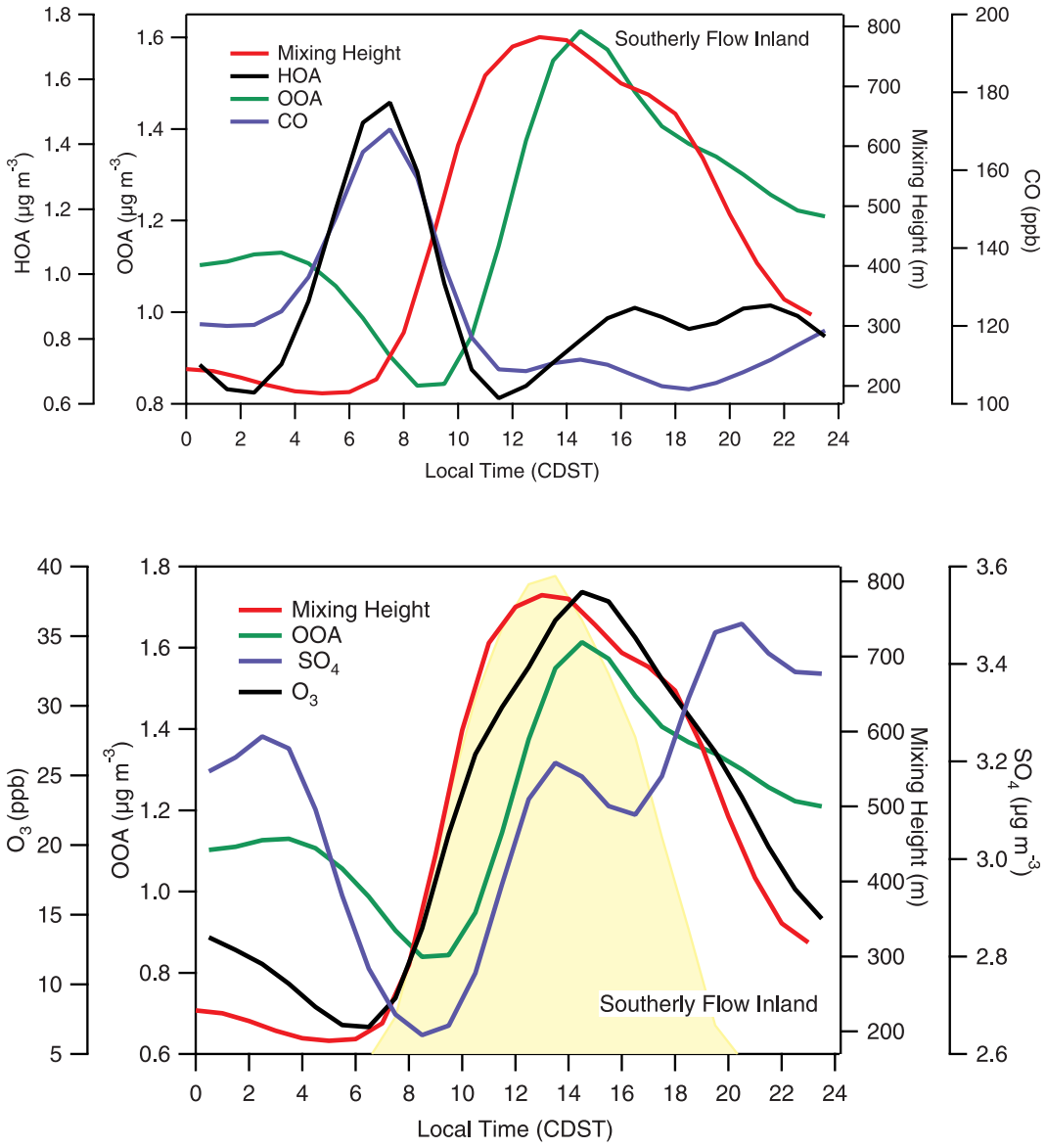

Figure 11. Diurnal cycles of OOA, hydrocarbon-like organic aerosol, CO, O_3, SO_4, and mixing height during periods of southerly inland flow. Solar radiation is shown in yellow.

industrial sources of HOA, elevated concentrations (Figure 11) in the early morning hours corresponded with morning rush hour traffic. HOA concentrations and CO mixing ratios then gradually decreased as the mixing height of the boundary layer increased. The mass size distribution of HOA had both Aitken and accumulation modes while OOA was largely confined to the accumulation mode (Figure 12). These size distributions showed little variation in magnitude or shape during the day, except for the elevated HOA Aitken mode during the morning rush hour. The dominant HOA Aitken mode in the mass size distribution especially during southerly flow (Figure 12) suggests that the HOA is a result of primary emissions. Conversely, the presence of OOA solely in the accumulation mode suggests a secondary aerosol formed from the condensation of semivolatile organic gases onto the existing aerosol surface area. The absence of an increase in OOA concentrations during the early morning hours under southerly flow is further evidence for a different source than that of HOA. Although OOA concentrations and ozone mixing ratios both increased during the day as a result of photochemical oxidation, the timing of the increases did not coincide and thus they were only weakly correlated (r^2 = 0.38). The increases in OOA concentrations and ozone mixing ratios during the day were likely from both in situ production and mixing from aloft as the mixing height of the boundary layer increased. OOA concentrations and ozone mixing ratios declined late in the day as photochemical production ceased and the boundary layer mixing height decreased (Figure 11) cutting off vertical mixing from above.

3.2.2. Sulfate Aerosol

[53] NR-NH_4^+ + NR-$SO_4^=$ was the dominant submicrometer aerosol component in all three air mass categories. Over the gulf 32 ± 21% of the total sulfur (SO_2 + $SO_4^=$) was in the form of SO_2 while over land 64 ± 23% (southerly flow

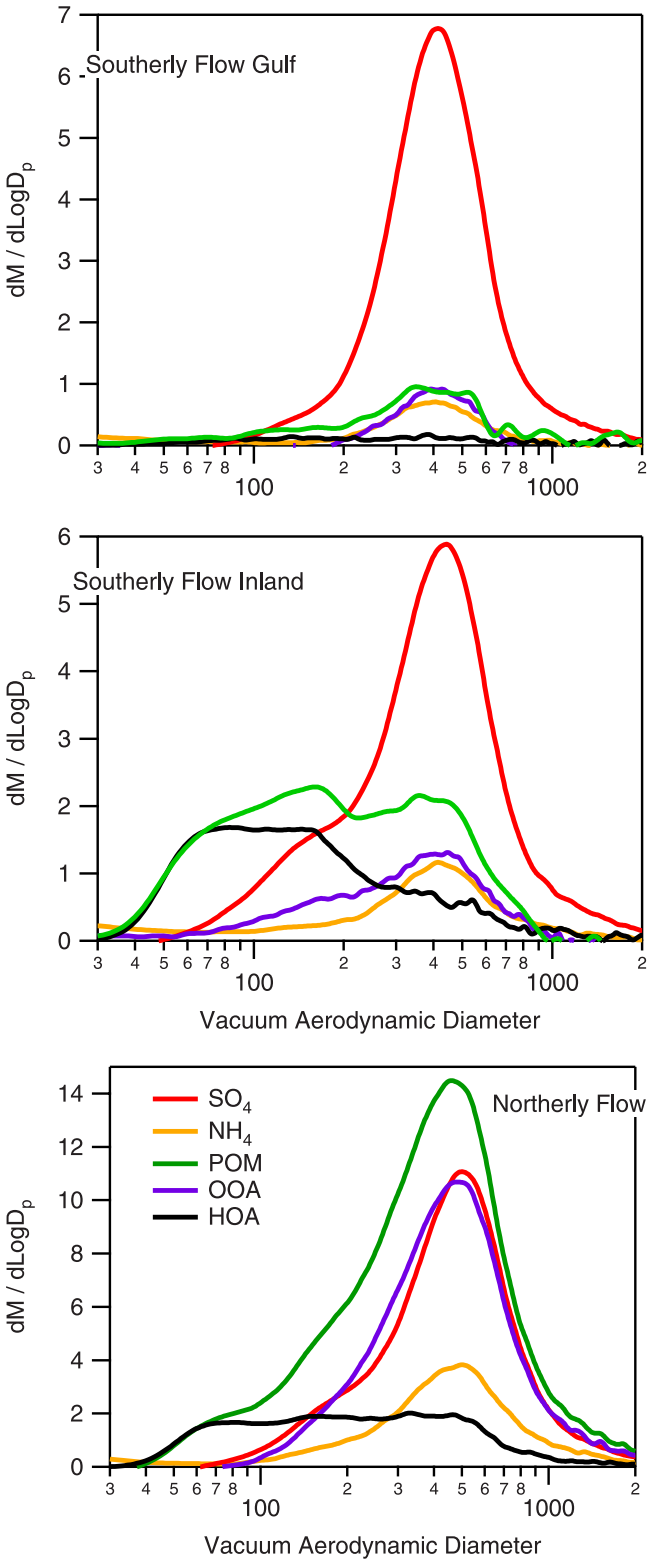

Figure 12. Mass size distributions of the dominant NR aerosol components measured by the quadrupole aerosol mass spectrometer.

inland) and 55 ± 25% (northerly flow) of the total sulfur was in the form of SO_2. Large SO_2 sources within the Houston/Galveston region include the Parish power plant (a coal-fired and natural gas-fired electric generation facility with no SO_2 gas scrubbers located in open farmland southwest of Houston), fossil fuel-fired electrical generation and process heat facilities along the Houston Ship Channel, and isolated large petrochemical complexes south of Houston [*Brock et al.*, 2003]. The petrochemical industries located along the Houston Ship Cannel and the Parish power plant were shown to be the predominant source of particle volume (mass) downwind of the Houston metropolitan area in 2000 [*Brock et al.*, 2003]. Particle number concentrations peaked immediately downwind of the sources while particle volume concentrations increased with distance from the source as SO_2 and other gases were oxidized to form aerosol mass [*Brock et al.*, 2003]. In a similar fashion, under northerly flow conditions during TexAQS/GOMACCS, the large point sources of SO_2 to the north of Houston and to the east and south of Dallas (e.g., Big Brown, Martin Lake, and Monticello electrical stations) could easily account for the NR-$SO_4^=$ concentrations (7.4 ± 4.8 μg m^{-3}) measured aboard the ship. The transit times on the order of 1–2 days would permit a large fraction of the emitted SO_2 to be converted to sulfate. During southerly flow inland periods (category 2), the SO_2 to total sulfur ratio was high, reflecting the local SO_2 sources. The NR-$SO_4^=$ concentrations (3.2 ± 2.4 μg m^{-3}), however, were only slightly higher than that measured over the Gulf (2.5 ± 1.1 μg m^{-3}) since the locally emitted SO_2 was too freshly emitted to have formed appreciable sulfate. The diurnal cycle of NR-$SO_4^=$ during the southerly flow inland periods was similar to that of OOA (Figure 11), decreasing during the night in the shallow stable boundary layer, increasing midmorning as the convective mixing of the boundary layer increased and then reaching an initial peak as the mixing height began to decrease late afternoon. Unlike OOA, however, the NR-$SO_4^=$ concentrations increased late in the day. We hypothesize that this is a result of advection of sulfate that was produced over the Gulf during the afternoon. A similar increase is not seen in ozone or OOA since their precursors were not abundant in the onshore flow.

[54] A key question, then, is what is the source of the elevated SO_2 and sulfate concentrations over the Gulf of Mexico in the "background" air (category 1) entering Texas? Biogenic dimethyl sulfide concentrations in the surface seawater off the coast of Texas averaged 2.4 ± 0.95 nM L^{-1}, a value typical of this latitude during the summer [*Bates et al.*, 1987]. Using the wind speeds measured at the ship and the *Nightingale et al.* [2000] wind speed/transfer velocity relationship, the flux of DMS to the atmosphere was 3.2 ± 2.6 μM m^{-2}d. Over the background marine atmosphere this flux supports an atmospheric sulfate concentration of 0.2–0.4 μg m^{-3} [*Bates et al.*, 2001], far less than that measured over the Gulf of Mexico. Another potential source of sulfate is the African continent as these air masses did contain high concentrations of dust. However, sulfate concentrations measured with dust in the submicrometer aerosol outflow of Africa were only 5–11% of the dust concentrations [*Bates et al.*, 2001; *Formenti et al.*, 2003], far less than that measured over the Gulf of Mexico. CO mixing ratios in this air mass (81 ± 14 ppbv) also suggest an absence of forest fire or urban pollution. A third potential source of sulfate is volcanic emissions. The FLEXPART back trajectories showed that some air masses sampled at the ship traveled through the Caribbean Sea and

may have passed over the Soufriere Hills Volcano on Montserrat Island. During July–September 2006 the average sulfur dioxide flux from the volcano was 200 t per day (The Montserrat Volcano Observatory, http://www.mvo.ms/) at an elevation of 1.1 km. While some of this SO_2 may have been mixed down into the marine boundary layer most of it will be transported in the free troposphere. There was no correlation of atmospheric sulfate concentrations measured at the ship with trajectories that had passed over Montserrat Island.

[55] A fourth potential source of the sulfate over the Gulf of Mexico is from marine vessel emissions. Emissions from marine vessels have gained increasing attention due to their significant local, regional, and global effects [*Corbett et al.*, 2007]. The corridor from the entrance to the Gulf of Mexico to Louisiana/Texas is a major shipping lane serving the Port of South Louisiana (New Orleans) and the Port of Houston, two of the ten busiest ports in the world by cargo volume (Gulf of Mexico Program, U.S. Environmental Protection Agency, http://epa.gov/gmpo/index.html). Recent ship emission inventories list the U.S. Gulf Coast emissions at 100,000 t of SO_2 per year [*Wang et al.*, 2008]. If this SO_2 is emitted into a 500m marine boundary layer over an area of 500,000 km^2 (a 200 nautical mile swath through the Gulf of Mexico to the Texas/Louisiana coast), with an atmospheric sulfur aerosol lifetime of one week, it would generate a concentration of 12 $\mu g\ m^{-3}$, more than 4 times the average concentration measured over the Gulf. The resulting aerosol would be acidic (measured ammonium to sulfate molar ratio was 0.79 ± 0.42) since the only source of ammonium ion is the ammonia emitted from the ocean [*Quinn et al.*, 1990]. Ship emissions also include high concentrations of nitrogen oxides (174,000 t expressed as NO_2 per year over the U.S. Gulf Coast) [*Wang et al.*, 2008]. Over the ocean, nitrogen oxides and their reaction products are absorbed onto the existing aerosol surface area and are thus generally found in the supermicrometer aerosol associated with dust or sea salt [*Bates et al.*, 2004]. The supermicrometer aerosol measured over the Gulf of Mexico was highly enriched in nitrate (15% of the total mass) and both the submicrometer and supermicrometer seasalt aerosols were depleted in chloride from the reaction with sulfuric and nitric acid vapors [*Bates et al.*, 2004]. Ship emissions, therefore, appear to be the major source of sulfate and nitrate over the Gulf of Mexico during TexAQS/GoMACCS.

4. Conclusions

[56] During most of August 2006, the boundary layer aerosol over the NW Gulf of Mexico advected into the region from the south and consisted of submicrometer (6.5 $\mu g\ m^{-3}$) NR-$SO_4^=$ and dust and supermicrometer (17.2 $\mu g\ m^{-3}$) sea salt and dust. Although this air mass had been over the Atlantic Ocean/Gulf of Mexico for 1–2 weeks, it was heavily impacted by continental (Saharan dust) and anthropogenic (ship) emissions. As the air mass entered southern Texas, local sources added an Aitken mode HOA rich aerosol. OOA and NR-$SO_4^=$ concentrations inland were lowest in the shallow, stable nocturnal boundary layer and increased during the day as the boundary layer mixing height increased, reflecting their secondary source. HOA concentrations and CO mixing ratios followed the opposite pattern, reflecting their primary source. Concentrations were highest in the early morning when the source was strong (automobile traffic) and mixing was limited (shallow, stable boundary layer) and then decreased during the day as the boundary layer mixing height increased.

[57] During September 2006 the boundary layer aerosol over southern Texas and the NW Gulf of Mexico advected into the region from the north and consisted of submicrometer (20.8 $\mu g\ m^{-3}$) NR-$SO_4^=$ and NR-POM and supermicrometer (7.4 $\mu g\ m^{-3}$) POM and dust.

[58] The integrated PM 2.5 mass at ambient RH includes the accumulation mode (primarily acidic sulfate and dust under southerly flow conditions) and part of the coarse mode (primarily sea salt, dust, and the acidic nitrate and sulfate absorbed by these basic components). The average PM 2.5 mass advecting into the Houston-Galveston area from the south during TexAQS 2006 was $20 \pm 12\ \mu g\ m^{-3}$. Air quality forecast models need to include ship emissions and dust transport to correctly characterize aerosol loadings in SE Texas. Compliance with PM 2.5 regulations in the Houston-Galveston area may require stricter controls on upwind aerosol sources (e.g., ship emissions).

[59] **Acknowledgments.** We thank the officers and crew of NOAA R/V *Ronald H. Brown* for their cooperation and enthusiasm and D. Hamilton, T.B. Onasch, J.D. Allan, and D.R. Worsnop for technical support. We thank J. Meagher, F. Fehsenfeld, and A.R. Ravishankara for programmatic support. This research was funded by the Atmospheric Constituents Project of the NOAA Climate and Global Change Program, the NOAA Office of Oceanic and Atmospheric Research, the NOAA Health of the Atmosphere Program and the Texas Air Quality Study. This is NOAA/PMEL contribution 3139.

References

Aiken, A. C., et al. (2008), O/C and OM/OC ratios of primary, secondary, and ambient organic aerosols with high resolution time-of-flight aerosol mass spectrometry, *Environ. Sci. Technol.*, *42*, 4478–4485.

Allan, J. D., J. L. Jimenez, P. I. Williams, M. R. Alfarra, K. N. Bower, J. T. Jayne, H. Coe, and D. R. Worsnop (2003), Quantitative sampling using an Aerodyne aerosol mass spectrometer: 1. Techniques of data interpretation and error analysis, *J. Geophys. Res.*, *108*(D3), 4090, doi:10.1029/2002JD002358.

Bates, T. S., J. D. Cline, R. H. Gammon, and S. Kelly-Hansen (1987), Regional and seasonal variations in the flux of oceanic dimethylsulfide to the atmosphere, *J. Geophys. Res.*, *92*, 2930–2938, doi:10.1029/JC092iC03p02930.

Bates, T. S., P. K. Quinn, D. J. Coffman, J. E. Johnson, T. L. Miller, D. S. Covert, A. Wiedensohler, S. Leinert, A. Nowak, and C. Neusüß (2001), Regional physical and chemical properties of the marine boundary layer aerosol across the Atlantic during Aerosols99: An overview, *J. Geophys. Res.*, *106*, 20,767–20,782, doi:10.1029/2000JD900578.

Bates, T. S., D. J. Coffman, D. S. Covert, and P. K. Quinn (2002), Regional marine boundary layer aerosol size distributions in the Indian, Atlantic, and Pacific Oceans: A comparison of INDOEX measurements with ACE-1, ACE-2, and Aerosols99, *J. Geophys. Res.*, *107*(D18), 8026, doi:10.1029/2001JD001174.

Bates, T. S., et al. (2004), Marine boundary layer dust and pollution transport associated with the passage of a frontal system over eastern Asia, *J. Geophys. Res.*, *109*, D19S19, doi:10.1029/2003JD004094.

Bates, T. S., P. K. Quinn, D. J. Coffman, J. E. Johnson, and A. M. Middlebrook (2005), The dominance of organic aerosols in the marine boundary layer over the Gulf of Maine during NEAQS 2002 and their role in aerosol light scattering, *J. Geophys. Res.*, *110*, D18202, doi:10.1029/2005JD005797.

Berner, A., C. Lurzer, F. Pohl, O. Preining, and P. Wagner (1979), The size distribution of the urban aerosol in Vienna, *Sci. Total Environ.*, *13*, 245–261, doi:10.1016/0048-9697(79)90105-0.

Brock, C. A., et al. (2003), Particle growth in urban and industrial plumes in Texas, *J. Geophys. Res.*, *108*(D3), 4111, doi:10.1029/2002JD002746.

Cahill, T. A., R. A. Eldred, and P. J. Feeney (1986), *Particulate monitoring and data analysis for the National Park Service, 1982–1985*, Air Qual. Group, Crocker Nucl. Lab., Davis, Calif.

Carrico, C. M., P. Kus, M. J. Rood, P. K. Quinn, and T. S. Bates (2003), Mixtures of pollution, dust, seasalt and volcanic aerosol during ACE-Asia: Light scattering properties as a function of relative humidity, *J. Geophys. Res.*, *108*(D23), 8650, doi:10.1029/2003JD003405.

Cheng, Y., B. Chen, H. Yeh, I. Marshall, J. Mitchell, and W. Griffeths (1993), Behavior of compact nonspherical particles in the TSI aerodynamic particle sizer model APS33B-Ultra-stokesian drag forces, *Aerosol Sci. Technol.*, *19*, 255–267, doi:10.1080/02786829308959634.

Corbett, J. J., J. J. Winebrake, E. H. Green, P. Kasibhatla, V. Eyring, and A. Lauer (2007), Mortality from ship emissions: A global assessment, *Environ. Sci. Technol.*, *41*(24), 8512–8518, doi:10.1021/es071686z.

Decesari, S., M. C. Facchini, E. Matta, F. Lettini, M. Mircea, S. Fuzzi, E. Tagliavini, and J. P. Putaud (2001), Chemical features and seasonal variation of fine aerosol water-soluble organic compounds in the Po Valley, Italy, *Atmos. Environ.*, *35*, 3691–3699, doi:10.1016/S1352-2310(00)00509-4.

de Gouw, J. A., et al. (2007), Sources of particulate matter in the Northeastern United States: 1. Direct emissions and secondary formation of organic matter in urban plumes, *J. Geophys. Res.*, *113*, D08301, doi:10.1029/2007JD009243.

Eatough, D. J., R. W. Long, W. K. Modey, and N. L. Eatough (2003), Semi-volatile secondary organic aerosol in urban atmospheres: Meeting a measurement challenge, *Atmos. Environ.*, *37*, 1277–1292, doi:10.1016/S1352-2310(02)01020-8.

Feely, R. A., G. J. Massoth, and G. T. Lebon (1991), Sampling of marine particulate matter and analysis by X-ray fluorescence spectrometry, in *Marine Particles: Analysis and Characterization*, *Geophys. Monogr. Ser*, vol. 63, edited by D. C. Hurd and D. W. Spencer, pp. 251–257, AGU, Washington, DC.

Formenti, P., W. Elbert, W. Maenhaut, H. Haywood, and M. O. Andreae (2003), Chemical composition of mineral dust aerosol during the Saharan Dust Experiment (SHADE) airborne campaign in the Cape Verde region, September 2000, *J. Geophys. Res.*, *108*(D18), 8576, doi:10.1029/2002JD002648.

Fuzzi, S., et al. (2006), Critical assessment of the current state of scientific knowledge, terminology, and research needs concerning the role of organic aerosols in the atmosphere, climate, and global change, *Atmos. Chem. Phys.*, *6*, 2017–2038.

Gerbig, C., S. Schmitgen, D. Kley, A. Volz-Thomas, K. Dewey, and D. Haaks (1999), An improved fast-response vacuum-UV resonance fluorescence CO instrument, *J. Geophys. Res.*, *104*(D1), 1699–1704, doi:10.1029/1998JD100031.

Grieshop, A. P., N. M. Donahue, and A. L. Robinson (2007), Is the gas-particle partitioning in alpha-pinene secondary organic aerosol reversible?, *Geophys. Res. Lett.*, *34*, L14810, doi:10.1029/2007GL029987.

Grund, C. J., R. M. Banta, J. L. George, J. N. Howell, M. J. Post, R. A. Richter, and A. M. Weickmann (2001), High-resolution doppler lidar for boundary layer and cloud research, *J. Atmos. Oceanic Technol.*, *18*, 376–393, doi:10.1175/1520-0426(2001)018<0376:HRDLFB>2.0.CO;2.

Harrison, R. M., and J. Yin (2000), Particulate matter in the atmosphere: Which particle properties are important for its effects on health?, *Sci. Total Environ.*, *249*, 85–101, doi:10.1016/S0048-9697(99)00513-6.

Holland, H. D. (1978), *The Chemistry of the Atmosphere and Oceans*, 154 pp., John Wiley, New York.

Huffman, J. A., J. T. Jayne, F. Drewnick, A. C. Aiken, T. Onasch, D. R. Worsnop, and J. L. Jimenez (2005), Design, Modeling, Optimization, and Experimental Tests of a Particle Beam Width Probe for the Aerodyne Aerosol Mass Spectrometer, *Aerosol Sci. Technol.*, *39*, 1143–1163, doi:10.1080/02786820500423782.

Intergovernmental Panel on Climate Change (IPCC) (2007), *Climate Change 2007: The Physical Science Basis. Contribution of Working Group I to the Fourth Assessment Report of the Intergovernmental Panel on Climate Change*, edited by S. Solomon et al., Cambridge Univ. Press, Cambridge, U.K.

Jaffrezo, J.-L., G. Aymoz, C. Delaval, and J. Cozic (2005), Seasonal variations of the water soluble organic carbon mass fraction of aerosol in two valleys of the French Alps, *Atmos. Chem. Phys.*, *5*, 2809–2821.

Jayne, J. T., D. C. Leard, X. Zhang, P. Davidovits, K. A. Smith, C. E. Kolb, and D. R. Worsnop (2000), Development of an aerosol mass spectrometer for size and composition analysis of submicron particles, *Aerosol Sci. Technol.*, *33*, 49–70, doi:10.1080/027868200410840.

Jimenez, J. L., et al. (2003), Ambient aerosol sampling using the Aerodyne Aerosol Mass Spectrometer, *J. Geophys. Res.*, *108*(D7), 8425, doi:10.1029/2001JD001213.

Jobson, B. T., C. M. Berkowitz, W. C. Kuster, P. D. Goldan, E. J. Williams, F. C. Fesenfeld, E. C. Apel, T. Karl, W. A. Lonneman, and D. Riemer (2004), Hydrocarbon source signatures in Houston, Texas: Influence of the petrochemical industry, *J. Geophys. Res.*, *109*, D24305, doi:10.1029/2004JD004887.

Kondo, Y., Y. Miyazaki, N. Takegawa, T. Miyakawa, R. J. Weber, J. L. Jimenez, Q. Zhang, and D. R. Worsnop (2007), Oxygenated and water-soluble organic aerosols in Tokyo, *J. Geophys. Res.*, *112*, D01203, doi:10.1029/2006JD007056.

Lanz, V. A., M. R. Alfarra, U. Baltensperger, B. Buchmann, C. Hueglin, and A. S. H. Prevot (2007), Source apportionment of submicron organic aerosols at an urban site by factor analytical modelling of aerosol mass spectra, *Atmos. Chem. Phys.*, *7*, 1503–1522.

Mader, B. T., et al. (2003), Sampling methods used for the collection of particle-phase organic and elemental carbon during ACE-Asia, *Atmos. Environ.*, *37*(11), 1435–1449, doi:10.1016/S1352-2310(02)01061-0.

Malm, W. C., J. F. Sisler, D. Huffman, R. A. Eldred, and T. A. Cahill (1994), Spatial and seasonal trends in particle concentration and optical extinction in the United States, *J. Geophys. Res.*, *99*, 1347–1370, doi:10.1029/93JD02916.

Marshall, I. A., J. P. Mitchell, and W. D. Griffiths (1991), The behavior of regular-shaped non-spherical particles in a TSI Aerodynamic Particle Sizer, *J. Aerosol Sci.*, *22*, 73–89, doi:10.1016/0021-8502(91)90094-X.

Matthew, B. M., T. B. Onasch, and A. M. Middlebrook (2008), Collection efficiencies in an Aerodyne aerosol mass spectrometer as a function of particle phase for laboratory generated aerosols, *Aerosol Sci. Technol.*, in press.

Nightingale, P. D., P. S. Liss, and P. Schlosser (2000), Measurements of air-sea gas transfer during an open ocean algal bloom, *Geophys. Res. Lett.*, *27*, 2117–2120, doi:10.1029/2000GL011541.

Orsini, D. A., Y. Ma, A. Sullivan, B. Sierau, K. Baumann, and R. J. Weber (2003), Refinements to the particle-into-liquid sampler (PILS) for ground and airborne measurements of water-soluble aerosol composition, *Atmos. Environ.*, *37*, 1243–1259, doi:10.1016/S1352-2310(02)01015-4.

Perry, K. D., T. A. Cahill, R. A. Eldred, D. D. Dutcher, and T. E. Gill (1997), Long-range transport of North African dust to the eastern United States, *J. Geophys. Res.*, *102*, 11,225–11,238, doi:10.1029/97JD00260.

Quinn, P. K., and D. J. Coffman (1998), Local closure during ACE 1: Aerosol mass concentration and scattering and backscattering coefficients, *J. Geophys. Res.*, *103*, 16,575–16,596, doi:10.1029/97JD03757.

Quinn, P. K., T. S. Bates, J. E. Johnson, D. S. Covert, and R. J. Charlson (1990), Interactions between the sulfur and reduced nitrogen cycles over the central Pacific Ocean, *J. Geophys. Res.*, *95*, 16,405–16,416.

Quinn, P. K., D. J. Coffman, V. N. Kapustin, T. S. Bates, and D. S. Covert (1998), Aerosol optical properties in the marine boundary layer during ACE 1 and the underlying chemical and physical aerosol properties, *J. Geophys. Res.*, *103*, 16,547–16,563, doi:10.1029/97JD02345.

Quinn, P. K., et al. (2000), Surface submicron aerosol chemical composition: What fraction is not sulfate?, *J. Geophys. Res.*, *105*, 6785–6806.

Quinn, P. K., D. J. Coffman, T. S. Bates, T. L. Miller, J. E. Johnson, E. J. Welton, C. Neusüss, M. Miller, and P. Sheridan (2002), Aerosol optical properties during INDOEX 1999: Means, variabilities, and controlling factors, *J. Geophys. Res.*, *107*(D19), 8020, doi:10.1029/2000JD000037.

Quinn, P. K., et al. (2004), Aerosol optical properties measured on board the Ronald H. Brown during ACE-Asia as a function of aerosol chemical composition and source region, *J. Geophys. Res.*, *109*, D19S01, doi:10.1029/2003JD004010.

Robinson, A. L., M. M. Donahue, M. K. Shrivastava, E. A. Weitkamp, A. M. Sage, A. P. Grieshop, T. E. Lane, J. R. Pierce, and S. N. Pandis (2007), Rethinking organic aerosols: Semivolatile emissions and photochemical aging, *Science*, *315*, 1259–1262, doi:10.1126/science.1133061.

Savoie, D. L., and J. M. Prospero (1980), Water-soluble potassium, calcium, and magnesium in the aerosols over the tropical North Atlantic, *J. Geophys. Res.*, *85*, 385–392, doi:10.1029/JC085iC01p00385.

Schauer, J. J., et al. (2003), ACE Asia intercomparison of a thermal-optical method for the determination of particle-phase organic and elemental carbon, *Environ. Sci. Technol.*, *37*, 993–1001, doi:10.1021/es020622f.

Schindler, D. W., S. E. M. Kasian, and R. H. Hessiein (1989), Biological impoverishment in lakes of the midwestern and northeastern United States from acid rain, *Environ. Sci. Technol.*, *23*, 573–580, doi:10.1021/es00063a010.

Seibert, P., and A. Frank (2004), Source-receptor matrix calculation with a Lagrangian particle dispersion model in backward mode, *Atmos. Chem. Phys.*, *4*, 51–63.

Stohl, A., and D. J. Thomson (1999), A density correction for Lagrangian particle dispersion models, *Boundary Layer Meteorol.*, *90*, 155–167, doi:10.1023/A:1001741110696.

Stohl, A., M. Hittenberger, and G. Wotawa (1998), Validation of the Lagrangian particle dispersion model FLEXPART against large scale tracer experiments, *Atmos. Environ.*, *32*, 4245–4264, doi:10.1016/S1352-2310(98)00184-8.

Sullivan, A. P., R. J. Weber, A. L. Clements, J. R. Turner, M. S. Bae, and J. J. Schauer (2004), A method for on-line measurement of water-soluble

organic carbon in ambient aerosol particles: Results from an urban site, *Geophys. Res. Lett.*, *31*, L13105, doi:10.1029/2004GL019681.

Sullivan, A. P., R. E. Peltier, C. A. Brock, J. A. de Gouw, J. S. Holloway, C. Warneke, A. G. Wollny, and R. J. Weber (2006), Airborne measurements of carbonaceous aerosol soluble in water over northeastern United States: Method development and an investigation into water-soluble organic carbon sources, *J. Geophys. Res.*, *111*, D23S46, doi:10.1029/2006JD007072.

Turpin, B. J., and H. Lim (2001), Species contribution to PM2.5 concentrations: Revisiting common assumptions for estimating organic mass, *Aerosol Sci. Technol.*, *35*, 602–610, doi:10.1080/02786820152051454.

Ulbrich, I. M., M. R. Canagaratna, Q. Zhang, D. R. Worsnop, and J. L. Jimenez (2008), Interpretation of organic components from positive matrix factorization of aerosol mass spectrometric data, *Atmos. Chem. Phys. Discuss.*, *8*, 6729–6791.

Wang, C., J. J. Corbett, and J. Firestone (2008), Improving spatial representation of global ship emissions inventories, *Environ. Sci. Technol.*, *42*, 193–199, doi:10.1021/es0700799.

Weber, R. J., D. Orsini, Y. Daun, Y.-N. Lee, P. Klotz, and F. Brechtel (2001), A particle-in-liquid collector for rapid measurement of aerosol chemical composition, *Aerosol Sci. Technol.*, *35*, 718–727, doi:10.1080/02786820152546761.

Whittlestone, S., and W. Zahorowski (1998), Baseline radon detectors for ship-board use: Development and deployment in ACE-1, *J. Geophys. Res.*, *103*, 16,743–16,751, doi:10.1029/98JD00687.

Winklmayr, W., G. P. Reischl, A. O. Lindner, and A. Berner (1991), New electromobility spectrometer for the measurement of aerosol size distributions in the size range 1 to 1000 nm, *J. Aerosol Sci.*, *22*, 289–296, doi:10.1016/S0021-8502(05)80007-2.

Zappoli, S., et al. (1999), Inorganic, organic and macromolecular components of fine aerosol in different areas of Europe in relation to their water solubility, *Atmos. Environ.*, *33*, 2733–2743, doi:10.1016/S1352-2310(98)00362-8.

Zhang, Q., M. R. Alfarra, D. R. Worsnop, J. D. Allan, H. Coe, M. R. Canagaratna, and J. L. Jimenez (2005), Deconvolution and quantification of hydrocarbon-like and oxygenated organic aerosols based on aerosol mass spectrometry, *Environ. Sci. Technol.*, *39*, 4938–4952, doi:10.1021/es048568l.

Zhang, Q., et al. (2007), Ubiquity and dominance of oxygenated species in organic aerosols in anthropogenically-influenced Northern Hemisphere midlatitudes, *Geophys. Res. Lett.*, *34*, L13801, doi:10.1029/2007GL029979.

W. M. Angevine, W. A. Brewer, B. L. Lerner, S. C. Tucker, and E. J. Williams, Chemical Sciences Division, Earth Systems Research Laboratory, NOAA, Boulder, CO 80309-0216, USA.

T. S. Bates, D. Coffman, P. K. Quinn, and K. Schulz, Pacific Marine Environmental Laboratory, NOAA, 7600 Sand Point Way NE, Building 3, Seattle, WA 98115, USA. (tim.bates@noaa.gov)

D. S. Covert and J. E. Johnson, Joint Institute for the Study of the Atmosphere and Ocean, University of Washington, Box 355672, Seattle, WA 98195, USA.

A. Stohl, Department of Regional and Global Pollution Issues, Norwegian Institute for Air Research, P. O. Box 100, N-2027 Kjeller, Norway.